

# Zero-shot Structure Learning and Planning for Autonomous Robot Navigation using Active Inference

Daria de Tinguy, Tim Verbelen, Emilio Gamba, Bart Dhoedt

**Abstract**—Autonomous navigation in unfamiliar environments requires robots to simultaneously explore, localise, and plan under uncertainty, without relying on predefined maps or extensive training. We present a biologically inspired, Active Inference-based framework, Active Inference MAPping and Planning (AIMAPP). This model unifies mapping, localisation, and decision-making within a single generative model. Inspired by hippocampal navigation, it uses topological reasoning, place-cell encoding, and episodic memory to guide behaviour. The agent builds and updates a sparse topological map online, learns state transitions dynamically, and plans actions by minimising Expected Free Energy. This allows it to balance goal-directed and exploratory behaviours. We implemented a ROS-compatible navigation system that is sensor and robot-agnostic, capable of integrating with diverse hardware configurations. It operates in a fully self-supervised manner, is resilient to drift, and supports both exploration and goal-directed navigation without any pre-training. We demonstrate robust performance in large-scale real and simulated environments against state-of-the-art planning models, highlighting the system’s adaptability to ambiguous observations, environmental changes, and sensor noise. The model offers a biologically inspired, modular solution to scalable, self-supervised navigation in unstructured settings. AIMAPP is available at <https://github.com/decide-ugent/AIMAPP>.

**Index Terms**—Autonomous Navigation, Active Inference, Cognitive Mapping, Predictive-coding, Topological Navigation, Planning, Bio-inspired, Robot Navigation, Mobile Robot,

## I. INTRODUCTION

The transition toward fully automated factories requires robots to be capable of autonomously exploring and navigating unfamiliar environments, a key challenge in robotics [1]–[3]. Navigation requires the integration of localisation, mapping, and planning into a coherent system. While each of these problems has been studied extensively in isolation, combining them into a robust and general-purpose framework remains challenging, particularly in large, dynamic, and partially observable environments. Classical approaches often suffer from high computational demands for real-time operation (a path-planning algorithm) [4], drift-prone odometry and metric maps (a SLAM method) [5], or heuristic strategies that lead to inefficient exploration and backtracking (a path planning method) [6]. Neural methods such as Neural-SLAM (a path planning and SLAM method) [7] improve flexibility but rely on extensive pre-training, which limits adaptability to new or dynamic environments.

One promising alternative to strategise path planning is the Active Inference Framework (AIF) [8], a computational model of perception and action rooted in neuroscience. Active Inference treats navigation as a process of probabilistic inference:

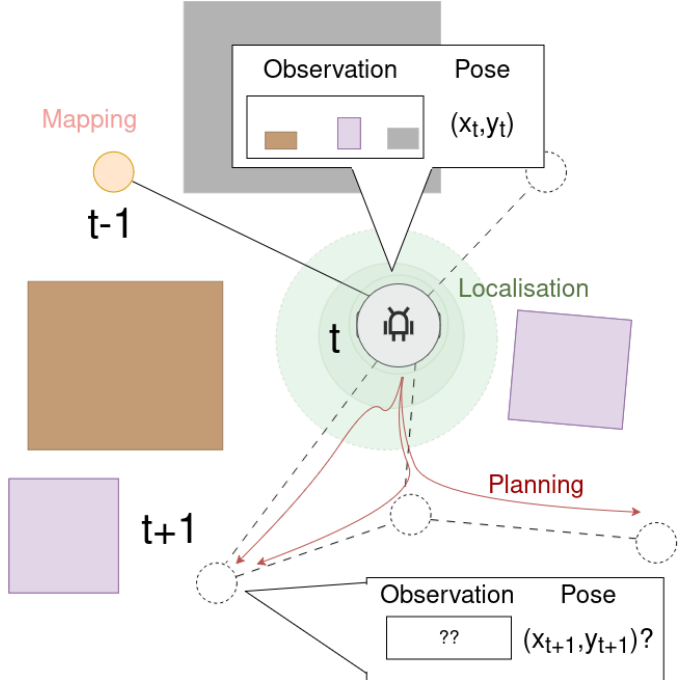


Fig. 1. Our model coarsely localises itself based on local motion and accumulated observations, remembering in a topological map where it has been and could potentially go. Planning follows Active Inference Principles, considering where the agent’s preferences lie (whether to gather information about the surroundings or reach a specific objective). Visited states (up to time  $t$  presented with coloured circles on the topological map) have a visual observation and a known position, while unvisited states (blank circles with dotted edges) hold a probable position and no observation. We plan through consecutive nodes in the topological graph to determine the next motion.

an agent maintains beliefs about the world, which can be reshaped based on new evidence, compares them to predicted future outcomes, and acts to minimise the mismatch between its predictions and sensory observations. In robotics, this translates into a unified framework where exploration and goal-directed navigation emerge naturally from the same underlying principle: reducing uncertainty about the environment while pursuing task-relevant states.

Building on this idea, we propose a bio-inspired navigation model, Active Inference MAPping and Planning (AIMAPP), coarsely presented in Figure 1, that maintains a sparse topological map linking sensory observations with metric localisation, and uses it to plan trajectories that balance information gain with goal efficiency. Unlike traditional artificial intelligence approaches, our system does not rely on pre-training, pre-defined map structures, or globally consistent metric representations [9]. Instead, it continuously adapts its beliefs from sensorimotor feedback, enabling robust performance in

ambiguous, dynamic, and partially observable environments. To keep planning tractable, the agent evaluates only relevant policies based on its current context [10]. Localisation is handled probabilistically rather than relying solely on odometry, ensuring resilience to drift. To move, the agent autonomously assigns and reassesses goals, balances exploration and exploitation, and recovers from most motion failures without requiring manual intervention.

AIMAPP exhibits the following key properties:

- Online learning: the agent incrementally updates its internal representation of the environment without requiring pre-training.
- Self-supervised learning: it autonomously determines how to navigate based on accumulated sensorimotor experience without requiring human intervention.
- Dynamic system modelling: the agent learns to model motion and transitions without assuming a fixed environmental structure, enabling generalisation to arbitrary, unknown environments.
- Robustness to uncertainty: localisation and decision making are Bayesian-based, allowing resilience to sensor drift and ambiguous inputs (aliased observations or change in environment).
- Data modality flexibility: any sensory input (e.g., RGB, depth, LiDAR) can be incorporated.
- Biological plausibility: the architecture draws inspiration from hippocampal functions such as episodic memory, place cells, and topological reasoning.
- Modularity: our approach can be integrated into existing navigation stacks in ROS-based systems and is fit for diverse navigation tasks (exploration or goal-reaching).
- Scalability: due to its sparse, topological map structure and belief-based planning, the model scales efficiently to large and high-dimensional spaces.

We evaluate our model in both simulated and real environments of varying scale and complexity. Results show that our Active Inference approach achieves exploration efficiency comparable to or exceeding state-of-the-art planning-based algorithmic methods (e.g., FAEL [11], GBPlanner [12], Frontiers [6]), while maintaining near-optimal coverage relative to human teleoperated exploration (90% Coverage Efficient -CE- overall runs). The system demonstrates robustness to moved obstacles in simulation and drift and sensor uncertainty in the real world, enabling reliable operation in real-world settings where our odometry-based baselines (e.g., Frontiers with Nav2 [13]) often failed. Moreover, exploration and goal-reaching are achieved within a single architecture, without task-specific re-tuning, across environments ranging from simulated houses and warehouses to real-world garages up to 325 m<sup>2</sup>.

Together, these contributions highlight the robustness, adaptability, and biological plausibility of Active Inference as a navigation strategy, bridging neuroscience-inspired theory and practical deployment in robotics. Rather than relying on globally accurate maps, our agent treats navigation as hypothesis testing: generating predictions about future states, evaluating them through action, and updating beliefs based on

surprise.

In the following sections, we review related work, present our Active Inference-based model for mapping, localisation, and decision-making, and evaluate its performance in terms of exploration, adaptation to moving obstacles, drift resistance, and goal-reaching.

## II. RELATED WORK

Robust and efficient autonomous navigation requires solving several interconnected challenges, including localisation, mapping, path planning, and obstacle avoidance. Traditional approaches have tackled these components with varying levels of integration and success. More recently, bio-inspired frameworks, particularly those based on Active Inference, have gained traction for their ability to provide flexible and adaptive navigation. In this section, we review key methodologies in three main categories: classical navigation systems, learning-based models, and biologically inspired approaches.

### A. Classical Navigation Systems

Classical navigation methods are often built upon metric mapping and localisation pipelines such as Simultaneous Localisation and Mapping (SLAM). There have been many notable examples, such as ORB3-SLAM [5] and many other notable approaches, such as depth-based SLAM [14], PLP-SLAM [15] and FAST-LIO2 [16], which leverage visual or LiDAR data for accurate pose estimation and mapping. These approaches excel in structured and uniformly lit conditions (especially LiDAR-based mappings), but they are prone to drift over time, even with loop closure, particularly in large or dynamic environments. Furthermore, many metric methods struggle with memory inefficiency and do not scale well to large unstructured worlds. Finally, SLAM primarily focuses on localisation and mapping, while path planning and obstacle avoidance require additional modules as indicated in [17]. Topological mapping offers an alternative to metrical maps, where the environment is represented as a graph of connected states rather than precise coordinates, as demonstrated in [18], [19]. This improves scalability and can better handle aliasing in perceptual input. However, many topological methods rely on heuristics for node creation and can be sensitive to environmental changes or perceptual noise.

### B. Learning-Based Navigation

With the rise of machine learning, many navigation systems now leverage deep neural networks to learn policies directly from data. Reinforcement Learning (RL), in particular, enables agents to acquire navigation and mapping skills through iterative interaction with the environment, improving decision-making under uncertainty, such as sensor noise and partial observability [2]. Neural network-based approaches (RL, Deep-RL...) offer advantages such as improved navigation performance (better exploration and more refined planning strategies), increased robustness to sensor noise, and reduced reliance on engineered features.

Some notable examples include Neural SLAM [7], which integrates cognitive mapping and policy learning in an end-to-end fashion to visually explore. Self-supervised methods such as BYOL [20], RECON [21], and ViKiNG [22], learn visual representations without explicit supervision but with months of collected data. NoMaD [23] uses a Transformer and diffusion model to jointly handle exploration and goal-reaching within a unified framework. Other approaches employ world models, such as [3], which uses latent Bayesian surprise to drive exploration, or [24], which predicts action outcomes and enables zero-shot manipulation. Zero-shot learning refers to the agent's ability to navigate without pre-training or prior exposure to the environment.

These methods often generalise well across visually similar environments and reduce dependence on human-designed features. However, they typically require large-scale offline training and curated datasets. Moreover, they usually struggle with knowledge transfer across environments, particularly in dynamic or large-scale settings. Most are also task-specific, trained either specifically for exploration [20], [21] or goal-reaching [22], [25]. NoMaD [23] is a notable exception, simultaneously addressing both tasks, but it remains limited to visual observations. In contrast, our approach supports any input modalities (bag-of-words, semantic labels, images, point clouds, etc.), though we only use visual observations as input in this work; the observation process is not considered part of the model.

### C. Bio-Inspired Navigation

Inspired by the cognitive processes of animals, bio-inspired navigation approaches integrate perception, memory, and decision-making in more adaptive ways. RatSLAM [26], for example, draws on principles from rodent hippocampal function to construct a topological cognitive map. It is effective at correcting drift and maintaining robust maps under uncertainty. However, it lacks autonomy in decision-making and goal-directed behaviour.

Other models like NNSLAM [7] incorporate neural networks for exploration and localisation, but require extensive visual training and struggle in unfamiliar scenarios. Bio-inspired neural networks have also been widely used in reactive collision-free navigation [27], but most systems assume static environments and lack probabilistic reasoning under uncertain situations.

Among bio-inspired methods, Active Inference has emerged as a unifying framework. Rooted in the principle that agents act to minimise Expected Free Energy (i.e. surprise), AIF treats navigation as inference rather than control. It integrates sensing, prediction, localisation, and planning into a single, adaptive generative process [8].

Several works have illustrated the use of AIF for navigating simulated mazes [28], [29] or simple structured environments [30], [31]. However, illustrations of navigating real environments with active inference are but a few. [32] demonstrates how combining AIF with imitation learning enables dynamic replanning and visual prediction in simple real-world scenarios, while GSLAM [33] fuses AIF and RatSLAM principles

to improve localisation and mapping in indoor environments. However, both methods require pre-training over, respectively, possible actions or observations and do not support full exploration in open-ended environments. They need to have previously defined the environment, usually requiring human intervention. Our model, inspired by AIF principles, operates in a zero-shot, online fashion, continuously learning from incoming sensory data without requiring prior training. The resulting model supports robust exploration, drift correction, and dynamic adaptation, demonstrating performance competitive with more classical path planning approaches while requiring fewer assumptions and no training resources.

### III. ACTIVE INFERENCE IN AIMAPP

The Active Inference Framework presents an interesting framework for understanding how organisms perceive and interact with their environment. Traditionally, biological agents have been thought to understand their environment by piecing together detailed information from sensory inputs [34], [35]. Continuously reconstructing the environment to track changes can be resource-intensive, particularly in fast-changing settings where quick decision-making is crucial for survival. Being able to reproduce such a mechanism would translate to more flexible and intuitive systems in robotics. AIF suggests that organisms are continually making predictions, a process akin to statistical inference, where they develop hypotheses or expectations about the actual state of their environment [36]. Our model adheres to the AIF principle, employing a mathematically grounded pipeline that remains fully interpretable, thereby explaining how agents interact, adapt, and navigate unstructured environments. It operates in a zero-shot, self-supervised, online-learning fashion: no pre-training is required, and sensory data is processed in real time to build and update an internal map of the environment.

The AIF framework is structured around three recurring steps:

- 1) Perception: inferring hidden world states from incoming observations.
- 2) Prediction and Action Selection: using a generative model to plan actions that either maximise task utility or reduce uncertainty about the model.
- 3) Learning: updating model parameters based on mismatches between expected and actual observations.

Our internal generative model is formalised as a partially observable Markov decision process (POMDP), enabling decision-making under uncertainty. At each step, the agent simulates possible action sequences (policies  $\pi$ ), in our case, using a Monte Carlo Tree Search (MCTS), scores them according to its current beliefs and goals, selects the most promising one, and executes the first action. Observations from the environment are then compared to predictions, and the model is updated accordingly. This continuous sense–predict–act–learn loop allows the agent to balance exploration and goal-seeking seamlessly.

We will first present our model before diving into each step of the process

### A. World Modelling

World models are an internal representation of the environment, generating predictions about possible future sensory information emitted by the environment. They are widely used for modelling abstract rules of the environment and allow the agent to predict the next state of the world based on the previous state and incoming action. The closer the rules of the world model match the real world, the better the agent's understanding of the consequences of its actions. Classically, worlds are modelled as a POMDP with, at any time  $t$ , the current observation  $o_t$  and determined past motion  $a_{t-1}$  from which we can infer state  $s_t$ , following Equation (1) where tildes ( $\tilde{\cdot}$ ) denote sequences over time.

$$P(\tilde{o}, \tilde{s}, \tilde{a}) = P(o_0|s_0)P(s_0) \prod_{t=1}^{\tau} P(o_t|s_t)P(s_t|s_{t-1}, a_{t-1}) \quad (1)$$

In this work, we deviate from the standard form by considering the latent state to be decomposed into two parts: a spatial position  $p_t$  and a state  $s_t$  (capturing particular information about a specific localisation defined by  $o$  and  $p$ ). This results in the extended generative model (2).

$$P(\tilde{o}, \tilde{s}, \tilde{p}, \tilde{a}) = P(o_0|s_0)P(s_0)P(p_0) \prod_{t=1}^{\tau} P(o_t|s_t, p_t)P(s_t, p_t|s_{t-1}, p_{t-1}, a_{t-1}) \quad (2)$$

In practice, calculating the true posterior  $P(o|s)$  is typically intractable, because the model evidence  $P(o)$  and the posterior probability  $P(s|o)$  cannot be computed [8]. Thus, we resort to variational inference, which introduces the approximate posterior  $Q$ . In our temporal model, it takes the form defined in Eq (3). The goal is to make  $Q(s)$  as close as possible to  $P(s|o)$ , which is achieved by minimising their Kullback–Leibler (KL) divergence.

$$Q(\tilde{s}, \tilde{p}|\tilde{o}, \tilde{a}) = Q(s_0, p_0|o_0) \prod_{t=1}^{\tau} Q(s_t, p_t|s_{t-1}, p_{t-1}, a_{t-1}, o_t) \quad (3)$$

How well this approximation fits the evidence can be measured by the Variational Free Energy (VFE) denoted  $F$ , defined in (4). Negative  $F$  is known as the Evidence Lower Bound (ELBO) in machine learning.

$$F_Q = \underbrace{D_{KL}[Q(\tilde{s}, \tilde{p}|\tilde{a}, \tilde{o})||P(\tilde{s}, \tilde{p}|\tilde{a}, \tilde{o})]}_{\text{posterior approximation}} - \underbrace{\log[P(\tilde{o})]}_{\text{log evidence}} \quad (4)$$

Minimising the KL divergence between the variational posterior  $Q$  and the true posterior  $P$  is equivalent to reducing the model's variational free energy  $F$ , which serves as a bound on the negative log-evidence (or "surprise") of the observations. In other words, minimising  $F$  increases the evidence the model has for its internal beliefs about the world, a process also known as maximising the ELBO.

This minimisation is equivalent to reducing the model's variational free energy  $F$ , which serves as a bound on the

negative log-evidence (or "surprise") of the observations. In other words, minimising  $F$  increases the evidence the model has for its internal beliefs about the world — a process also known as maximising the Evidence Lower Bound (ELBO).

Through this mechanism, the agent continually updates its internal beliefs to select the approximate posterior that best explains its past and current sensory inputs, aligning perception and action toward reducing uncertainty.

In the next subsection, we extend this classical formulation to our specific generative model used throughout this work.

### B. Model Specification

Our specific approximate posterior distribution defined in Equation (3) relies on priors (previous states and known structure of the world, either deduced or given) and observations to localise the agent within its environment. The presented model works with the following essential distributions:

- State transitions ( $B_s$ ): Likelihood of the agent moving between states.
- Position transitions ( $B_p$ ): Likelihood to move between positions.
- Observation likelihoods ( $A_o$ ): How likely certain observations are at each state.
- Position likelihoods ( $A_p$ ): The likelihood of being in a particular position at each state.

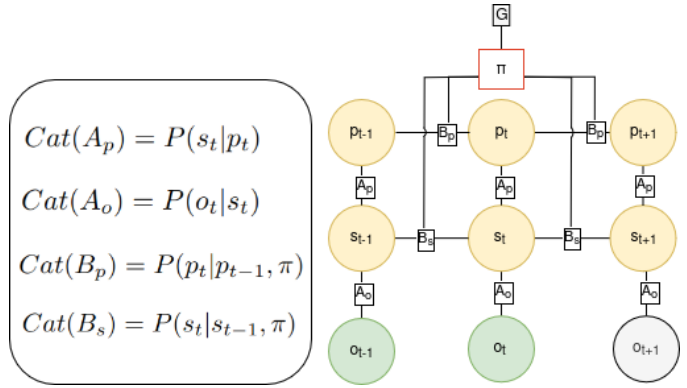


Fig. 2. POMDP of our model.  $\text{Cat}$  stands for Categorical. The model integrates states ( $s_t$ ), positions ( $p_t$ ), and observations ( $o_t$ ) over time, guided by policies ( $\pi$ ) and expected free energy ( $G$ ). The categorical distributions define transition and observation likelihoods:  $A_p$  (position likelihoods),  $A_o$  (observation likelihoods),  $B_p$  (position transitions), and  $B_s$  (state transitions). This structure underpins the inference scheme in Equation (3), enabling the agent to infer hidden states and positions from sensory observations and prior beliefs.

Figure 2 visually explains our POMDP process, where  $G$  refers to Expected Free Energy (EFE), which allows us to evaluate and select future policies  $\pi$  (series of actions) that will be applied as actions  $a$ . The process to obtain  $G$  will be discussed in the next section.

### C. Predicting the Next States and Decision-Making

According to the Free Energy Principle, agents must minimise free energy to form a model that best explains their environment [8]. For perception, this principle is implemented by minimising VFE during inference, as previously explained.

For action and planning, the same principle extends into the future: agents should act to minimise the EFE  $G$  under their candidate policies.

Formally, a policy  $\pi$  is a sequence of future actions. The expected free energy  $G(\pi)$  quantifies how well following  $\pi$  is expected to reduce surprise [28]. It decomposes into two complementary contributions:

- **Exploration (epistemic value):** expected information gain reducing uncertainty about the environment.
- **Exploitation (pragmatic value):** expecting to reach a preferred observation, such as a specific target object (e.g. "food").

This decomposition illustrates that exploration and exploitation are not separate objectives bolted onto the model, but emerge naturally from minimising EFE. Behaviour can thus be understood in the same way as, for example, a rat in a maze [37]: sometimes venturing into unknown corridors to learn about the environment (uncertainty reduction), and sometimes returning to rewarding locations (preference fulfilment). In both cases, behaviour emerges from balancing curiosity with goal-directed action.

Practically, we first define the potential policies from the current localisation through a greedy MCTS strategy [38], [39]; definition and pseudo code are available in Appendix A-C. This approach incrementally builds a search tree by simulating possible action sequences and focusing computation on the most promising branches, considering EFE over policies. This yields three main advantages over predefined or exhaustive policy sets: 1) Scalability, as it avoids combinatorial explosion in large or continuous action spaces, 2) Adaptability, which dynamically prioritises policies relevant to the agent's current context, and 3) Efficiency, which limits computation to policies that meaningfully differ in their predicted outcomes.

To determine the most relevant policy at any time  $t$ , we assess all policies through a softmax transformation (5).

$$P(\pi) = \sigma(-\gamma G(\pi) - H) \quad (5)$$

where  $\sigma$  is the softmax function and  $\gamma$  is a precision parameter (inverse temperature) controlling action stochasticity. Higher values of  $\gamma$  bias the agent towards policies with minimal expected free energy, while lower values promote greater randomness in action selection.

A general issue with prediction over future steps, without relying on hierarchical structures, is that the further into the future the prediction lies, the more diluted the probabilities become. That is why we introduce an inductive term  $H$  [40] in our policy evaluation. This term allows us to consider pragmatic values from states over the horizon range of the policies. It adds weight to actions leading toward those preferred states and propagates this information from those states to adjacent nodes up to our current state. For a more in-depth comprehension of this term, refer to Appendix A-B.

The EFE  $G$  of a particular policy is computed through  $G(\pi)$  presented in Equation (6).

$$G(\pi) = \sum_{\tau} G(\pi, \tau) \quad (6)$$

where  $\tau$  indexes consecutive steps of the future policy.

To determine  $G$  we balance epistemic values (information gain) over future states (how much can we learn about a state) and parameters (how much can we update our model) with pragmatic values (utility term), considering possible preferences on observations, poses or states (respectively  $C_o$ ,  $C_p$  and  $C_s$ ). The inference of  $G$  step by step in the future is detailed in Equation (7) considering multiple elements. To fully understand the mechanism of our model, we decoupled the collision perception  $c$  from the observation  $o$ , however, fundamentally, the collision knowledge stems from observation  $o$ . In fact, the probability of encountering an obstacle  $P(c_{\tau})$ , measured as a binary probability (1 or 0, respectively there is a risk of collision or not) over the preference  $C_c$  of not encountering an obstacle, has a major impact on the policy viability.

$$\begin{aligned} G(\pi, \tau) &= \mathbf{E}_{Q_{\pi}} [\log Q(s_{\tau}, p_{\tau}, A_p | \pi) - \log Q(s_{\tau}, p_{\tau}, A_p | c_{\tau}, \pi) \\ &\quad - \log P(c_{\tau} | C_c) - \log P(o_{\tau} | C_o) \\ &\quad - \log P(p_{\tau} | C_p) - \log P(s_{\tau} | C_s)] \\ &= \underbrace{\mathbf{E}_{Q_{\pi}} [\log Q(s_{\tau}, p_{\tau} | c_{\tau}, o_{\tau}, \pi) - \log Q(s_{\tau}, p_{\tau} | \pi)]}_{\text{expected information gain on states (inference)}} \\ &\quad - \underbrace{\mathbf{E}_{Q_{\pi}} [\log Q(A_p | s_{\tau}, p_{\tau}, c_{\tau}, o_{\tau}, \pi) - \log Q(A_p | s_{\tau}, p_{\tau}, \pi)]}_{\text{expected information gain on parameters (learning)}} \\ &\quad - \underbrace{\mathbf{E}_{Q_{\pi}} [\log P(c_{\tau} | C_c)] - \underbrace{\mathbf{E}_{Q_{\pi}} [\log P(o_{\tau} | C_o)]}_{\text{utility term on observation}}}_{\text{expected collision}} \\ &\quad - \underbrace{\mathbf{E}_{Q_{\pi}} [\log P(p_{\tau} | C_p)] - \underbrace{\mathbf{E}_{Q_{\pi}} [\log P(s_{\tau} | C_s)]}_{\text{utility term on state}}}_{\text{utility term on position}} \end{aligned} \quad (7)$$

The expected information gain quantifies the anticipated shift in the agent's belief over the state from the prior (e.g.  $Q(s_{\tau} | \pi)$ ) to the posterior (e.g.  $Q(s_{\tau} | c_{\tau}, o_{\tau}, \pi)$ ) when pursuing a particular policy  $\pi$ . On the other hand, the utility term assesses the expected log probability of observing a preferred outcome under the chosen policy. This value intuitively measures the likelihood of the policy guiding the agent toward its preferences. Free Energy indirectly encourages outcomes that align with its preferences or target states. This approach makes the utility term less about "reward" in the traditional sense of Reinforcement Learning and more about achieving coherence with the agent's preferences.

#### D. Updating the model

Having determined how the agent infers its state and selects actions, we now describe how it practically updates its internal parameters in light of inferred poses, current and expected observations. This learning step closes the perception-action-learning loop, enabling the agent to refine its world model so that it continues to explain sensory observations accurately.

In essence, the agent compares its current generative model, as defined by parameters governing pose likelihoods ( $A_p$ ), observation likelihoods ( $A_o$ ), and state transitions ( $B_s$ ), against an expanded model incorporating newly predicted or observed states [10]. The goal is to determine whether the expanded

model better explains the environment. This comparison applied to  $A_p$  is quantified by the change in free energy,  $\Delta F$ , shown in Equation 8:

$$\Delta F = F[\tilde{A}_p(\theta)] - F[A_p(\theta)] \quad (8)$$

Here,  $\tilde{A}_p$  represents the updated pose likelihood model, and  $\theta$  its parameters. If  $\Delta F$  is negative (meaning the new model has lower free energy), the agent updates its internal structure  $A_p$  to incorporate the newly encountered (or predicted) information.

When a new state is confirmed or predicted, the pose model  $A_p$  is expanded, triggering corresponding updates to the pose transition tensor  $B_p$  and to all other state-related matrices. The updated observation model  $A_o$  assigns uniform probabilities to unvisited states, reflecting initial uncertainty (high entropy, low  $P(s_t)$ ). The transition model  $B_s$  is also adapted to connect new states with existing ones. This is done via a Dirichlet pseudo-count update, with a learning rate that depends on whether the trajectory was imagined or physically experienced, and whether it was deemed feasible or impossible (details in Appendix A-A).

A similar mechanism applies during inference when a novel sensory input is encountered. In this case, only  $A_o$  is expanded, since the update pertains to the observation dimension rather than the state dimension.

By continuously applying this update process, the agent maintains an adaptable, self-consistent world model that integrates both real and imagined experience. This ensures that exploration not only extends the map but also improves the accuracy of navigation when pursuing specific goals.

#### IV. ROBOTIC INTEGRATION

AIMAPP was implemented in a physical agent during navigation. It covers mapping, localisation and planning.

Having introduced the generative model in Section III-A, we will now discuss how minimising free energy in a robotics context yields mapping and localisation.

##### A. Mapping

Mapping in our framework is grounded in Active Inference. The agent maintains a generative model linking states  $s$  (locations), positions  $p$  (metric displacements), and observations  $o$  (sensory inputs such as visual panoramas). It updates its internal generative model to minimise expected free energy, allowing it to predict unexplored regions and infer the structure of the environment. Concretely, EFE drives the trade-off between exploiting familiar states (goal-directed path planning) and enriching the map when predictions about observations are uncertain or surprising. This dynamic process gives rise to a cognitive map, an internal representation inspired by biological navigation systems [41]–[45]. Cognitive maps support flexible navigation and spatial reasoning, capturing both the layout of the environment and the agent’s experience within it.

In our approach, the cognitive map is implemented as a topological graph containing metric information, where nodes represent distinct agent states ( $s$ ), each corresponding to a

spatial location ( $p$ ) with an associated observation ( $o$ ). Metric information is retained locally for each node, enabling approximate spatial reasoning without requiring globally consistent coordinates. The map grows adaptively as the agent explores, adding new states when new poses are expected in given directions, supporting scalability to large or dynamic environments.

*a) Node creation and connectivity:* New nodes are created when a motion leads to a predicted position  $p_t$  exceeding a radius of influence from existing states. This expansion step comes from a discrepancy between the current model parameters  $A_p$  and expected model parameters  $\tilde{A}_p$  if we were to move to that new position, as defined in our EFE Eq (7) expected information gain on parameters and Eq (8), estimating that discrepancy.

The discrete set of available actions (e.g., 12 headings plus a “stay” action) defines the potential connectivity. This process is illustrated in Figure 3: each state can spawn neighbours only when motion carries the agent outside the influence zone of previous nodes, ensuring sparse but informative coverage.

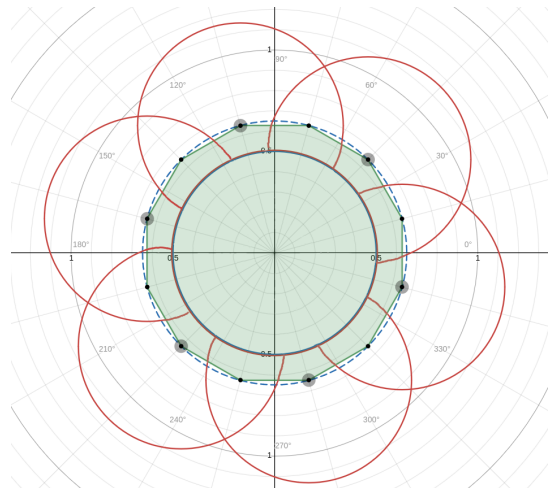


Fig. 3. Influence of a node at position (0,0) on adjacent node creation for an influence radius of 0.5 m and 12 discrete headings spanning 360°. Red circles represent the influence radius of each newly created node. The blue dashed circle marks the robot’s radius, including a padding term to account for its physical size (important near walls). The 12 black dots correspond to the midpoints of the 12 possible action directions. Dots with a black aura indicate valid positions where a new node can be created while respecting the minimum distance constraint (red radius) of adjacent nodes. Dots without an aura represent invalid positions (too close to an existing node) and could instead be created farther away (e.g., at 1 m). This arrangement allows the agent to maintain open junctions for future node expansion.

*b) State representation and observations:* Observations are stored as 360° panoramas stitched from consecutive camera frames (Figure 4). Each node encodes a coarse spatial position and a panoramic visual observation. The incoming observations are compared to stored visual memories using the Structural Similarity Index (SSIM) to determine familiarity. If no match is found, this signals either a novel location or a significant environmental change. The process of integrating observations into the map is illustrated in Figure 4. In the figure, we have a forward-facing camera; the robot turns to capture consecutive images of its surroundings. They are then stitched together to form a panorama.

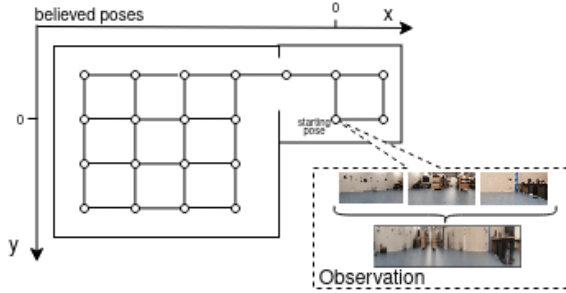


Fig. 4. schematic of what could be the topological map in a simple 2-room environment. Dots are states, or nodes, each state containing a  $360^\circ$  panorama obtained through stitching images together and associated with a position. Links between nodes are plausible transitions.

*c) Updating the generative model:* This learned map provides the base for localisation. Inference over hidden states  $s$  amounts to finding the most plausible node in the graph that explains the current observation  $o_t$  and predicted motion. If we are confident in our current state  $s_t$  (considering our VFE compared to a threshold defined in Appendix A-A), the likelihood matrix  $A_o$  is updated to associate the current observation with the believed state, improving robustness against perceptual aliasing and minor visual variations and reducing future surprise. However, if its Variational Free Energy confidence is low, the agent prioritises re-localisation, searching for familiar observations before updating the model.

*d) Sensory and motion agnosticism:* AIMAPP is designed to be modular: it accepts recognised observations from any perception system and relies on a motion controller to report goal-directed stops. This allows interchangeable components within the architecture, as shown in Figure 5. While resilient to moderate visual changes (lighting, small object displacements), the current panoramic-based approach struggles in highly dynamic environments where structural elements frequently change. Additionally, goal locations defined using panoramas may become invalid if the scene is no longer visually accessible. Prior work [46] explores lower bounds of visual place recognition and potential avenues for more robust sensory encoding. Future extensions could replace panoramic images with semantic or symbolic encodings (e.g., object categories or textual cues [47], [48]) to improve robustness in dynamic environments or reach objectives given specific objects' characteristics or names.

## B. Localisation

Given the topological map built during exploration, localisation is the inference step of Active Inference: determining which state  $s_t$  in the map best explains the current observation  $o_t$  and motion prediction  $P(p_t|p_{t-1}, a_{t-1})$ . Rather than depending solely on raw odometry or sensor data, the agent relies on its beliefs, i.e. the posterior distribution over states resulting from combining predicted motion with sensory evidence. This belief-driven approach makes localisation an active process of minimising free energy through perceptual inference (inferring  $s_t$ ), updating beliefs  $s$  with new evidence  $o$  and triggering

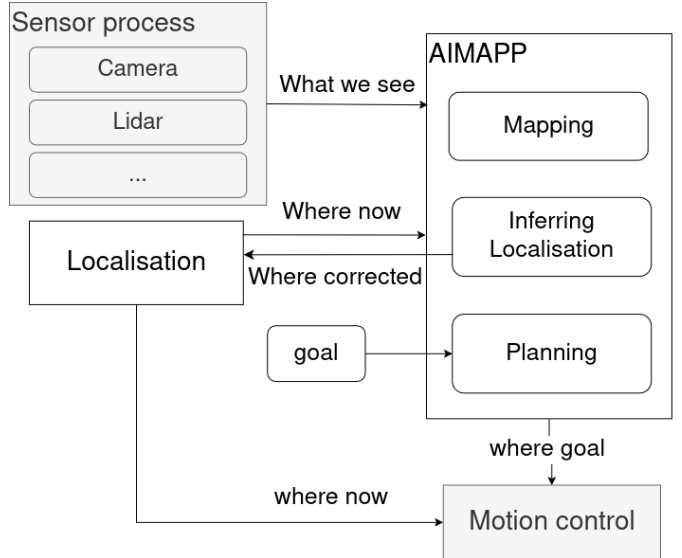


Fig. 5. Overview of the system architecture. In grey, we have modules that any ROS-compatible solution can replace. Modules interact through belief propagation. Inferring and planning (localisation, mapping and action selection) rely on the AIF framework. The perceptual and motion planning still use traditional approaches. Believed odometry takes precedence over sensor data. Preferences (goal) are expected from the user if we want to reach a target observation.

a full goal-oriented navigation with a preference to known observations when uncertain about its localisation.

A key implication of this design is that internal localisation is robust to drift. Since the agent prioritises consistency between predicted and observed outcomes, the exact physical position is less critical than whether its internal model correctly explains the sensory data. In familiar areas, mismatches caused by odometry drift can be corrected by recognising stored observations. In unexplored areas, however, drift cannot be directly corrected, and the agent must rely on its generative model to maintain consistency until additional information becomes available.

To illustrate this, consider the scenario in Figure 6. The agent starts at state  $s_0$  with observation  $o_0$  at position  $p_0$ . It intends to move forward 1m, but due to drift, it actually moves 2m. Its model, however, creates a new state  $s_1$  at  $p_1 = p_0 + 1m$ , consistent with the intended motion rather than the true displacement. After moving back 1m (without drift), the agent expects to be at  $s_0$ . At this point, it faces an inference problem: which state best explains the current observation?

Depending on its confidence in motion and observation, four outcomes are possible:

- Figure 6 1) the belief update favours prediction. We have a high confidence in motion toward  $p_0$  and observation, the agent recognises  $o_0$  even though it is not exactly at the right position, infers it is at  $s_0$ , and updates its belief accordingly (drift remains uncorrected physically, but the model is internally consistent).
- Figure 6 2) posterior shifts toward perceptual evidence. We have low confidence in motion, high confidence in observation  $o_1$ : the agent recognises  $o_1$ , infers it is at  $s_1$ , and updates its belief over motion to match perception.

The agent is believed to be at position  $p_1$ , in this simple example, the drift would be corrected.

- Figure 6 3) EFE encourages exploration. A low confidence in the current position  $o_1$  and observation  $o_0$ : the agent has a high uncertainty about its location, it will be considered lost when  $P(s_t)$  is low (given a threshold set by the user and described in Appendix A-A). The agent will enter an exploratory phase, seeking consecutive familiar observations to re-localise.
- Figure 6 4) update  $A_o$  matrix for known state  $s$ . A low confidence in observation (we don't recognise the observation) but high confidence in position  $p_0$ : the agent assumes it is at  $s_0$  but fails to recognise the input. It therefore adds a new observation to  $s_0$ , refining the observation model to account for variability (e.g., changes in lighting). The previous observation is not replaced; both are linked to the same state.

This belief-centred localisation shows how Active Inference principles naturally lead to flexible handling of odometry errors, perceptual aliasing, and uncertainty. The system does not simply "trust" sensors, but instead continuously evaluates which internal model best explains its sensory history.

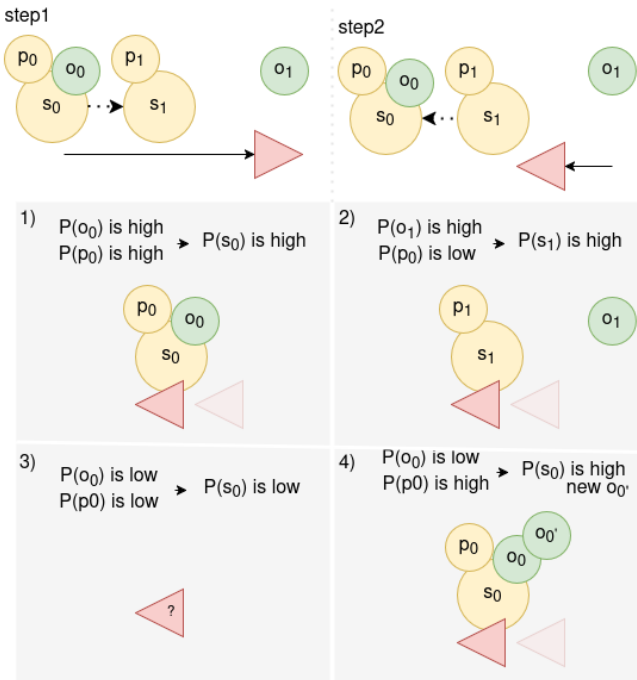


Fig. 6. Impact of drift on the agent's localisation. The top row illustrates the scenario: the red triangle is the agent; the solid line shows the true trajectory; the dashed line shows the trajectory perceived through odometry; the yellow circles are inferred states; the green circles are observations. The agent intends to move 1m right from  $s_0$  but actually moves 2m. Its model creates state  $s_1$  at the perceived position, while the true observation  $o_1$  belongs to the real position. On the next step, the agent moves 1m left (without drift) and expects to return to  $s_0$ . At this point, four localisation outcomes are possible: 1) High confidence in motion and observation: recognises  $o_0$ , infers  $s_0$ , updates belief (drift remains physically uncorrected). 2) Low confidence in motion, high confidence in observation: recognises  $o_1$ , infers  $s_1$ , updates belief accordingly. 3) Low confidence in both: cannot localise, enters the exploratory phase until a familiar observation is encountered. 4) High confidence in position, low confidence in observation: assumes  $s_0$  but fails to match input; adds a new observation ( $o'_0$ ) to  $s_0$ , expanding the observation model.

## V. RESULTS

We evaluate our framework across both simulated and real-world environments to assess its exploration efficiency, robustness to sensing, motion errors, and capacity for goal-directed navigation. Results are organised into three parts. First, we examine exploration performance, focusing on coverage efficiency compared to baseline approaches. Second, we study how the agent adapts to obstacles and odometric drift, highlighting differences between simulation and real-world trials. Finally, we evaluate goal-reaching behaviour, both in terms of qualitative strategy and quantitative success rates.

### A. Exploration

1) *Coverage*: We evaluated AIMAPP in four simulated environments and three real-world settings. The simulated setups included a mini ( $36\text{ m}^2$ ), small ( $80\text{ m}^2$ ), and large ( $280\text{ m}^2$ ) warehouse inspired by the Amazon Gazebo environment [49], and a  $175\text{ m}^2$  house environment [50] without doors, featuring kitchens, playrooms, and bedrooms. Both warehouses and houses contained challenging objects for LiDAR-based detection, such as curved chairs and forklifts. The real-world experiments were performed in 1) a small, fully controlled  $20.3\text{ m}^2$  bedroom environment with drift-inducing flooring, 2) a controlled  $185\text{ m}^2$  warehouse, and 3) a large  $325\text{ m}^2$  sandy parking lot where moving cars occasionally altered the navigable space (navigation was paused while cars crossed). Environment layouts are provided in Appendix C.

Across all scenarios, the agent began exploration from multiple initial positions. Since our model does not construct a metric map, we associated LiDAR range measurements with internal state representations to evaluate exploration.

We compared our approach (12m range 2D LiDAR + cameras, Nav2 for motion control) to several heuristic or algorithm-based exploration strategies that do not require pre-training:

- Frontier-based exploration [6], using a LiDAR and Nav2 SLAM [51].
- Gbplanner, an enhanced version of the 2021 DARPA SubT Challenge winner [52], combines Voxblox [53] with a topological map for 3D exploration planning.
- FAEL [11], based on frontier logic, with 3D mapping via UFOMap [54] and topological navigation.
- Manual exploration, a human teleoperated the robot around while NAV2 SLAM cartographed the surroundings.

Sensor setups varied substantially: Frontiers required a single 2D LiDAR, while our model also used a camera (in our work, the obstacle distance  $c$  was extracted from the LiDAR sensor instead of our visual observation  $o$  due to the lack of depth or stereo in our data. This dissimilarity has no impact on the model); FAEL used a 3D LiDAR, and Gbplanner used three cameras and two 3D LiDARs. For fairness, all models could use their sensors up to 12m (be it 2D or 3D LiDARs). All simulated experiments used a Turtlebot3 Waffle, except FAEL (Jackal [55]). Real-world trials used a RosbotXL [56] with an 18m range LiDAR (which was also restricted to a 12m range for comparable results). Additional details about the

models and robots are in Appendix D-A and B, respectively. Because AIMAPP is a zero-shot learning agent, we did not compare against learning-based methods [20], [21] requiring pre-training, which would have had unfair prior knowledge of the environments.

*a) Simulation Results:* The average coverage efficiency of each model, measured as explored area relative to distance travelled, averaged over five successful trials, is reported in Figure 7. Failures and human interventions are documented in appendix D-C. As a summary, we observed that Gbplanner was the most robust algorithm (87% success rate), followed by our model (79% success rate, comprising all simulated and real environments); FAEL is the model requiring the most human interventions.

Human explorations ("Manual" in Figure 7) are considered near-optimal, as the human has a general understanding of the whole layout and map while navigating. With this assumption in mind, we can compare Coverage Efficiency (CE) against teleoperated navigation. CE is a coefficient obtained by dividing the area covered (in  $m^2$ ) by the travelled distance (in m); time in seconds is not considered, as it largely depends on the motion-planning parameters (wheel speed) rather than the decision-making process. AIMAPP achieved near-optimal coverage compared to FAEL, Gbplanner and manual exploration, with an exploration efficiency 90.3% that of the manual motion, based on results shown in Table I. Overall, these results confirm that our model achieves consistently high coverage efficiency and normalised coverage progression across simulated and real environments, performing comparably to FAEL and often surpassing GBPlanner. In contrast, Frontiers consistently underperformed, highlighting the limitations of heuristic frontier-based strategies in cluttered or partially observable environments. Gbplanner methods valorise safe exploration paths, often wasting distance performing redundant back-and-forth movements before expanding to new zones. Frontiers performed worst, as it repeatedly attempted to reach unreachable frontier cells, wasting significant travel distance. These outcomes reflect the design intent of each method: AIMAPP and FAEL emphasise exploration efficiency, Gbplanner is tailored for robust subterranean exploration where narrow passages dominate and allow for human intervention in the navigation, while Frontiers is a well-known lightweight heuristic model.

A consistent plateau at approximately 90% coverage gain was observed in AIMAPP. This arose because the model prioritised updating nearby unvisited states already represented in its internal graph, rather than extending exploration beyond current detection range. As a result, node refinements occurred without proportional increases in spatial coverage. In smaller environments ( $\leq 80m^2$ ), all methods converged to similar performance levels (see Appendix D-B).

*b) Real-world Results:* In real-world trials, only AIMAPP and Frontiers could be deployed, as FAEL and Gbplanner required sensors unavailable on the physical platform. Both were tested from five different starting positions in the warehouse environment, which contained two long aisles and a large open area.

Our model consistently achieved faster coverage than Front-

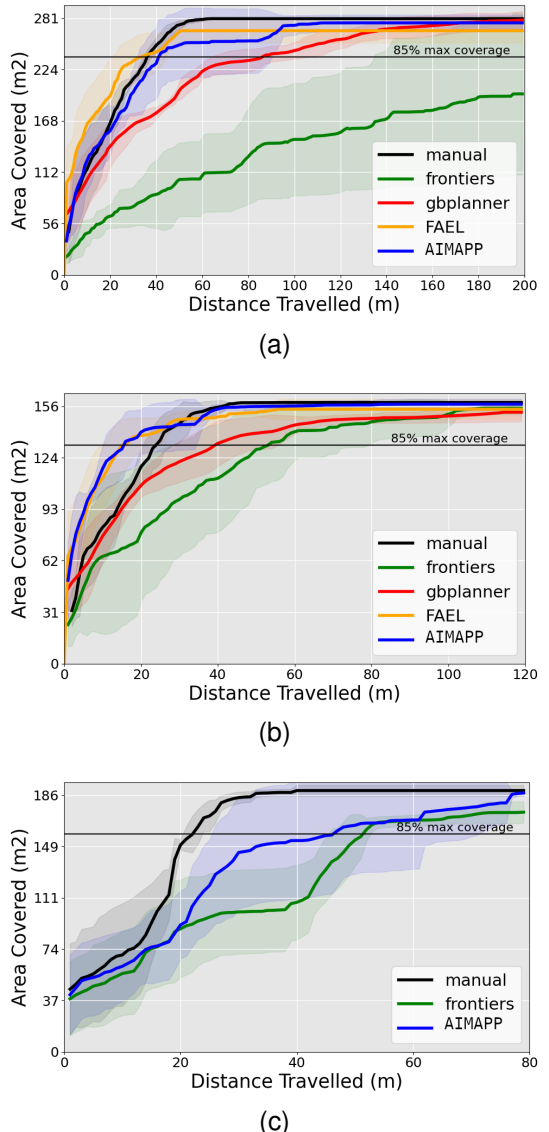


Fig. 7. Coverage efficiency of each model in the largest warehouse and home, as well as Frontiers and AIMAPP in a real warehouse, considering the agent's travelling distance.

TABLE I  
EXPLORATION EFFICIENCY METRICS ACROSS ENVIRONMENTS. CE: COVERAGE EFFICIENCY ( $m^2/m$ ), nAUC: NORMALISED AREA UNDER COVERAGE CURVE. VALUES ARE MEAN  $\pm$  STD OVER 5 RUNS.

Env.	Model	CE	nAUC
Simulated Large Warehouse	Manual	$4.25 \pm 0.43$	$0.55 \pm 0.02$
	AIMAPP	$4.02 \pm 1.24$	$0.62 \pm 0.06$
	Frontiers	$0.60 \pm 0.35$	$0.53 \pm 0.15$
	FAEL	$4.65 \pm 0.45$	$0.77 \pm 0.07$
	GBPlanner	$1.13 \pm 0.17$	$0.56 \pm 0.04$
Simulated House	Manual	$4.02 \pm 0.74$	$0.70 \pm 0.08$
	AIMAPP	$4.89 \pm 1.10$	$0.87 \pm 0.10$
	Frontiers	$2.18 \pm 0.15$	$0.77 \pm 0.17$
	FAEL	$5.23 \pm 1.90$	$0.79 \pm 0.06$
	GBPlanner	$3.70 \pm 0.15$	$0.50 \pm 0.04$
Real Warehouse	Manual	$4.89 \pm 0.53$	$0.65 \pm 0.09$
	AIMAPP	$2.68 \pm 0.40$	$0.70 \pm 0.10$
Real Warehouse	Frontiers	$2.11 \pm 0.52$	$0.62 \pm 0.15$

tiers, as presented in Figure 7c and Table I. The difference stemmed from strategy: AIMAPP efficiently moved between

unexplored regions, while Frontiers repeatedly revisited the same aisles due to attraction toward removed frontier cells (yet not using the unvisited aisle to plan going there). Performance varied with initial placement, reflecting the strong influence of warehouse geometry.

Interestingly, Frontiers performed somewhat better in the real warehouse than in the simulated warehouse or house of similar dimensions, likely because long aisles are more forgiving for its greedy strategy. Conversely, AIMAPP performed slightly less efficiently in the real warehouse than in simulation, as LiDAR detection errors occasionally caused it to attempt reaching unreachable goals, introducing inefficiencies in motion planning.

Exploration in the parking lot can be found in appendix D-B. While this environment is dynamic, we did not experiment with the obstacle avoidance performance of the motion planning, as it is not part of the model. When a change occurred in the environment (namely, a car moving around), the robot's motion was paused.

### B. Obstacles and Drift

AIMAPP dynamically adapts to changes in the environment during navigation by continuously updating its internal topological map. This process is illustrated in Figure 8 in a small-scale environment where the position of a box changes. As the agent moves and attempts transitions, it incrementally weakens the likelihood of inaccessible paths and reinforces the plausibility of reachable ones. Failed attempts to move toward an obstructed location trigger significant updates to the agent's belief structure, while successful access reinforces existing transitions. This adaptive behaviour enables rapid reconfiguration of the model in response to environmental shifts. For instance, in Figure 8b, state 7 becomes inaccessible after being blocked by the box. Consequently, all transitions leading to it are suppressed as the agent gathers evidence by navigating around the obstacle. For numerical details regarding the belief update mechanism, refer to Appendix A-A. The mechanism is agnostic of the environment, be it simulated or real; however, in the real world (namely, the parking lot), maps showing this process are blurred by motion drift. The effective task to contour a dynamic obstacle relies on our motion planning module, which was either a potential field or Nav2 in our experiments. They are not considered part of the proposed model.

*a) Drift Measurement:* To quantify drift under controlled conditions, we conducted experiments in a 185 m<sup>2</sup> warehouse equipped with Qualisys motion-capture cameras providing ground-truth odometry. These cameras were used exclusively for benchmarking and were not available to any navigation model. The trajectories estimated by our model, the robot's onboard sensor odometry, and the ground truth can be qualitatively compared in Figure 9. Missing segments correspond to gaps in Qualisys coverage.

The Root Mean Square Error (RMSE) on the  $x$  and  $y$  axes are reported in Table II, averaged across five successful runs. While the mean error of AIMAPP (1.83m) is similar to that of Frontiers (1.68m), the variance is substantially lower

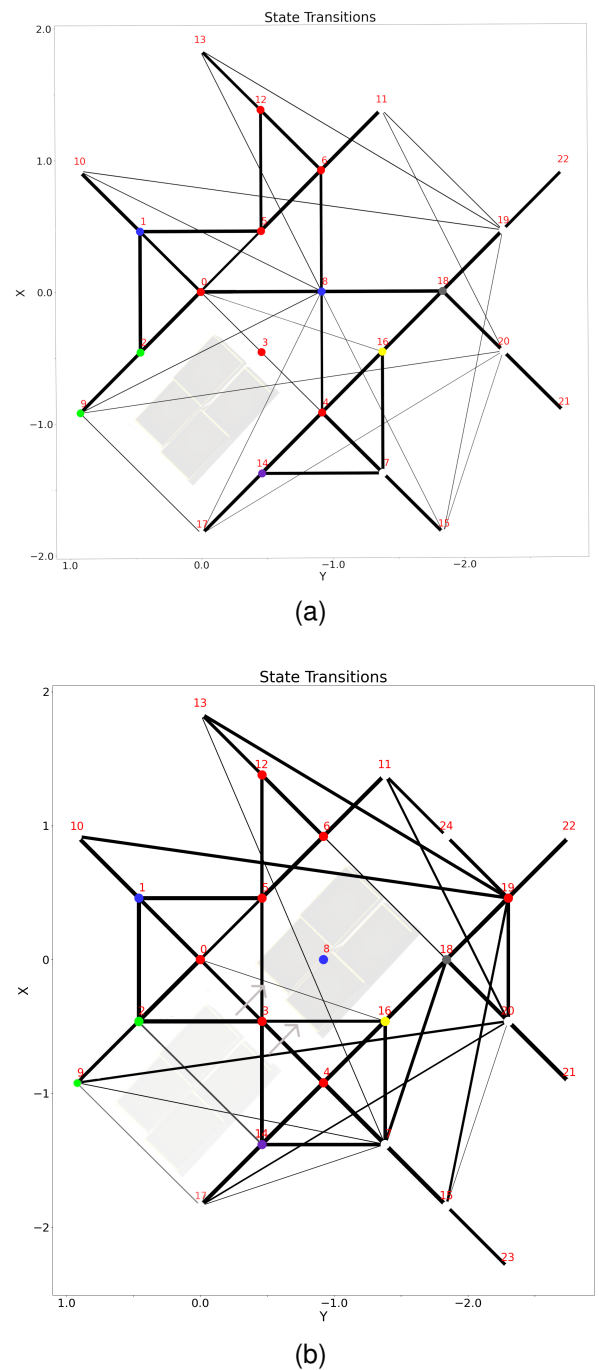


Fig. 8. The environment can adapt to change in real-time, here a box was displaced from (a) (-1,0) to (b) (0,-1) during exploration of a 25m<sup>2</sup> environment to rapidly demonstrate (in twenty steps taken around the box) how the map weakens impossible transitions and enforces previously improbable links. If pertinent, new nodes would be created.

( $\pm 0.77$ m vs.  $\pm 2.00$ m). This indicates that our approach produces consistently reliable trajectories, whereas Frontier-based exploration exhibits high variability, occasionally resulting in very poor localisation. The stability of our model brings it closer to the manual exploration lower bound ( $1.40 \pm 0.25$  m), which had a faster exploration, thus less opportunity to drift, suggesting that AIMAPP delivers competitive drift performance and greater robustness across repeated runs.

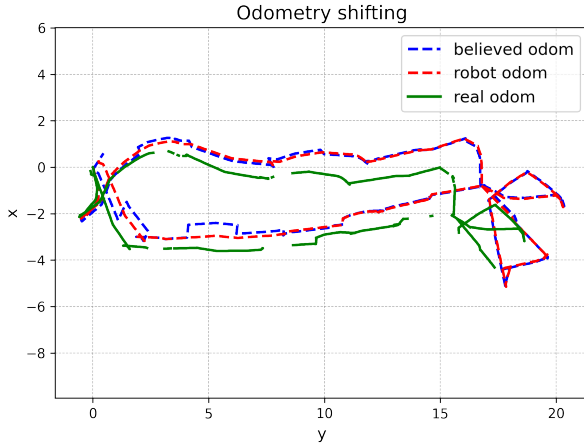


Fig. 9. Drift comparison in the  $(x, y)$  plane between our agent's internal belief (model odometry), the robot's onboard sensor odometry, and the ground-truth trajectory measured with Qualisys. Missing segments in the plot correspond to gaps in ground-truth perception.

TABLE II  
RMSE OVER X AND Y AVERAGED OVER 5 RUNS PER MODEL.

	AIMAPP model	AIMAPP sensor	Frontiers sensor	Manual sensor
RMSE (x,y)	$1.83 \pm 0.77$	$1.65 \pm 0.79$	$1.68 \pm 2.00$	$1.40 \pm 0.25$

A more pronounced distinction emerged in real-world conditions prone to severe drift. In environments with uneven terrain (such as parking lot) or changing flooring (house with both wood and carpet), wheel slippage led to large odometry errors which we could not quantitatively measure. While our model's belief-driven map gradually lost metric alignment with the ground truth, it remained operational: the agent could continue exploring and reliably reach goal observations. Moreover, the system tolerated temporary sensor failures; when odometry, camera, or LiDAR streams were restarted after a failure, the agent resumed operation without requiring reinitialisation. By contrast, Frontier-based exploration, relying on Nav2, failed under these conditions: once drift accumulated, maps became inconsistent and unusable, restarting the odometry was not an option, preventing further navigation. Consequently, no quantitative comparison with Frontiers was possible in the house or garage scenarios.

In summary, AIMAPP achieves drift performance comparable to that of ground truth odometry in controlled environments and demonstrates superior robustness under severe real-world conditions where baseline methods often fail. Its ability to remain functional, even with misaligned maps or sensor resets, highlights the practical resilience of the framework. However, future work should address long-term metric consistency for industrial usage.

### C. Goal Reaching

Beyond exploring and mapping its environment, a key requirement for autonomous agents is reliably reaching specified goals despite uncertainty in sensing, motion, or environmental changes. We evaluated how AIMAPP leveraged its internal belief and planning mechanisms to select and follow paths

toward desired observations. We first illustrate the conceptual strategy underlying goal-directed navigation, showing how the agent prioritises states and sequences that maximise expected utility. This is then followed by a quantitative assessment of performance, highlighting efficiency, robustness, and the ability to cope with real-world challenges such as drift, change in the environments, and partial observability.

a) *Goal-Directed Navigation Strategy*: In those experiments, we gave visual observations seen during exploration as the preferred observation  $C_o$  to reach. With a weight of 10 on the pragmatic value, to encourage the agent toward desiring this goal over exploration.

In our framework, goal-directed navigation emerges from the same Active Inference principles that drive exploration. While exploration favours previously unobserved states for their potential information gain, goal pursuit biases the agent toward states likely to generate a desired observation, given as input by the user.

Crucially, this preference only influences behaviour if the agent can imagine a feasible trajectory toward these states during planning. Indeed, far-removed high-utility states (desired objectives) that do not appear in the planning horizon of the MCTS would not guide navigation. To address this, we employ an inductive prior  $H$  (Formally introduced in Equation (5) and (10)), which spreads utility along sequences of plausible actions leading to the goal. This mechanism allows the agent to evaluate paths rather than single states, effectively assigning intermediate states a utility based on their potential to reach the target observation, even outside its planning horizon.

In this way, the planning algorithm favours sequences of actions that are most likely to lead to successful goal attainment, even if the terminal goal states are not presently imagined from the current position.

This process is illustrated in Figure 10, in a simulated large warehouse. Heatmaps show the evolving utility of paths over five planning steps. Initially (step 0), the agent is biased in the correct general direction, despite the goal states (circled green) not yet being pictured. As the agent transitions to step 1, intermediate states leading toward the goal increase in utility, while states in the opposite direction are suppressed. This iterative process continues through steps 2-4: at each step, the agent updates its belief over state transitions and refines its utility estimates, progressively converging toward the goal state cluster. The agent's trajectory demonstrates how probabilistic generative models under Active Inference can support robust zero-shot planning in partially explored environments. The use of the inductive prior ensures that even distant or initially unimagined goals can influence immediate action selection, producing efficient, coherent, and biologically plausible navigation behaviour. At each step, the agent simultaneously updates its positional belief through re-localisation and evaluates future trajectories, maintaining flexibility in response to newly encountered information. This stepwise propagation of utility resembles "place cell firing" in the hippocampus, where spatial locations associated with expected sensory outcomes become activated before the agent physically reaches them [57]. By integrating predicted observations with trajectory planning, the agent can dynamically

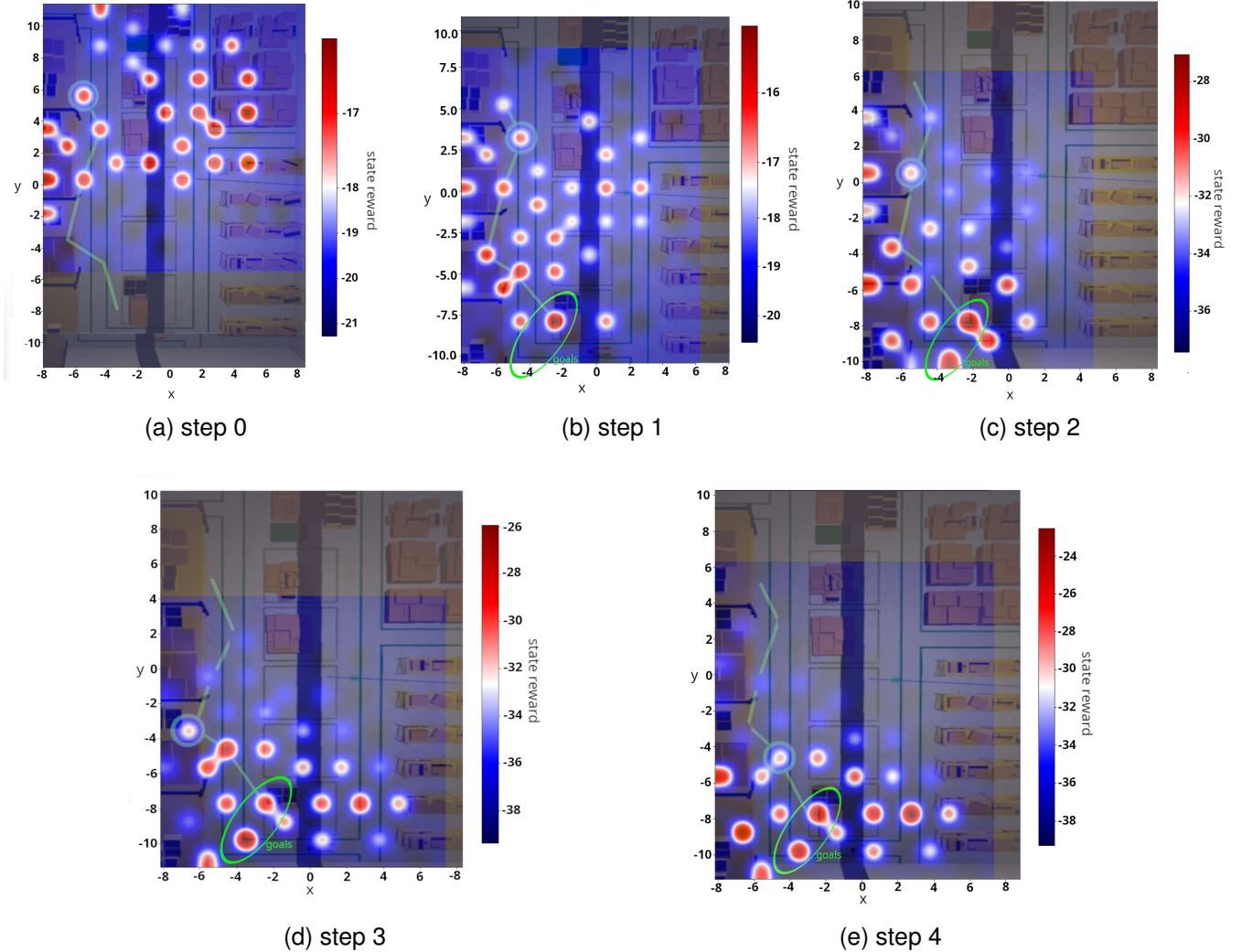


Fig. 10. MCTS path "states rewards" (free energy minimisation) considering an observation held by two states (circled green on figures). The higher the value, the more attractive the place. The agent went from the starting pose, circled green in step 0, to a state holding the desired observation in 5 steps. The full path of the agent is presented in dark green, and its current location is circled in dark green. We can see the zone attractivity of the path as the agent moves. In a) step 0, we see that the agent is attracted toward the correct direction even before it can imagine the goal state.

select actions that maximise the likelihood of reaching desired sensory states while accounting for uncertainty in partially mapped environments.

In the situation where we give an unknown desired observation to reach the agent, the model will show a preference over unvisited states until it finds a matching observation, resulting in a behaviour akin to exploration. Thus, all our tests have been realised in partially explored environments where the goal has been observed during the exploration phase to clearly differentiate the exploration from the goal-reaching behaviour.

*b) Quantitative Goal Reaching and Robustness in Real and Simulated Environments:* Having illustrated how the agent plans and propagates utility to reach a target observation in a step-by-step demonstration, we now evaluate the quantitative performance of this goal-directed navigation. This includes measuring path efficiency and the agent's ability to maintain near-optimal behaviour across both simulated and real-world

environments.

To quantitatively assess goal-directed navigation, we measured the path length taken by the agent relative to the optimal path distance, computed using the A\* algorithm over the agent's topological graph. The A\* path assumes perfect knowledge of transitions and serves as a benchmark for ideal goal-reaching performance. This evaluation is not perfect as deviations from this baseline naturally occur when the agent initially overestimates the feasibility of a transition. Upon encountering an invalid transition, the model updates its beliefs and re-plans around the obstacle, resulting in longer, but necessary, detours that are not considered by A\*. The same mechanism handles newly encountered obstacles during execution, reflecting the agent's capacity for adaptive replanning. We realised 40 goal-reaching runs in all environments with goals of various distances from the agent's starting position, presented in Figure 11. We assumed the agent had prior knowl-

edge of its starting position to avoid the re-localisation steps the agent would need to identify its location. Average path lengths across all trials indicate that the agent's performance remains close to the optimal A\* benchmark. Across all runs, the agent achieved an average deviation of  $0.9m \pm 1.48m$  from the ideal path, indicating low variability in goal-reaching performance. Relative deviations averaged  $13.8\% \pm 23.2\%$ . The mean efficiency was approximately 91%, demonstrating that the agent typically journeyed only 9% further than the optimal path. Furthermore, the agent reached the goal within 20% of the ideal distance in 73% of trials, highlighting robustness even in the presence of drift (in real environments only) or unexpected obstacles. As long as the goal observation was recognised by the model, no run failed to reach its location except in two cases we will detail.

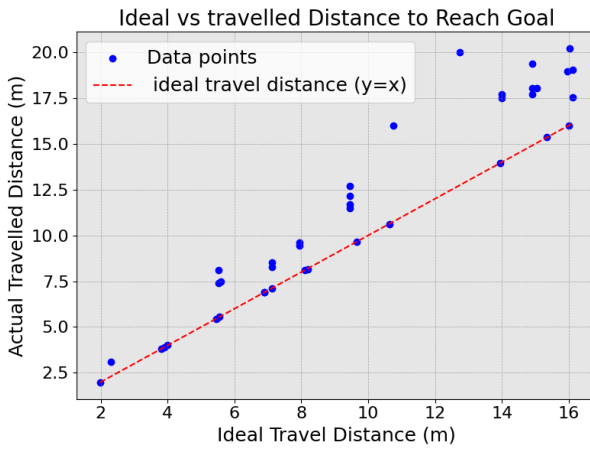


Fig. 11. Travelled distance to goals vs A\* expected distance from robot position to closest goal image position across all environments.

Three representative paths from a fixed starting location to the same goal (Figure 12a) in a simulated environment are shown in Figure 12c. Across all trials, the agent successfully reaches the target observation, prioritising transitions with high expected utility. Slightly longer paths are sometimes preferred to maintain higher confidence in expected outcomes, consistent with the Active Inference principle that action selection balances efficiency with belief consistency.

In real-world trials, the agent was evaluated in three environments of varying complexity: a small controlled bedroom, a structured warehouse, and a semi-structured parking lot. Figure 12d illustrates the taken trajectories in the parking lot to reach the goal presented in Figure 12b. Despite challenges such as sensor drift, changes in the environments (car' presence between exploration and goal-reaching runs may have changed), and varying lighting conditions, the agent successfully reached its goals in nearly all runs (15 out of 17 runs over all environments). When initial localisation errors or unexpected obstacles occurred, belief updates and replanning allowed the agent to correct its course, as illustrated by minor detours in the green trajectory.

Across the seventeen real-world goal-reaching experiments, only two failures occurred: one in the house environment, caused by severe drift resulting in a wrong re-localisation and

having the goal far beyond a wall, and one in the parking lot, where the robot's holonomic wheels became physically stuck in sandy terrain. These edge cases underscore the limits of AIMAPP to drift in clamped areas and the impact of physical limitations on the navigation.

Overall, the agent demonstrates robust, near-optimal goal-directed navigation across both simulated and real-world settings. Deviations from optimal paths are reasonable and interpretable, arising primarily from belief estimations and updates or environmental constraints. These results confirm the efficacy of our MCTS and AIF-based planning with inductive utility propagation, showing that the agent can achieve reliable zero-shot navigation while balancing efficiency and robustness in partially explored environments.

#### D. AIMAPP Computational Scalability

To evaluate the scalability of AIMAPP, we measured its computational footprint in terms of memory usage and runtime performance on a Jetson Orin Nano platform.

*a) Model size and memory usage:* Model size was assessed by serialising its parameters into a .pkl file across 31 independent runs over time. The number of stored states had no measurable effect on model size, confirming that the state-space representation remains lightweight even as the map grows. The dominant memory factor is the storage of RGB panoramic observations. Model size (in Megabits -MB-) scales linearly with the number of stored observations, following:

$$\text{Model size (MB)} \approx 1.32 \times (\text{number of observations}) + 0.17.$$

The largest model contained 36 unique observations and required only 44.9 MB, demonstrating that AIMAPP remains memory-efficient even with heavy observation data.

*b) Runtime and resource usage:* Runtime performance was profiled over the same 31 navigation runs on the Jetson Orin Nano (15V power, Jetpack 6.1, Ubuntu 22.04, ROS2 Humble). During each run, AIMAPP operated concurrently with the Nav2 stack, camera drivers, plotting, and logging processes (saving model at a periodic interval). The average system resource consumption was  $47.5\% \pm 16.8\%$  CPU and  $36.8\% \pm 2.2\%$  RAM. Of this, Nav2 accounted for approximately 30% of CPU usage, which remained stable across all trials. At no point did computation exceed platform capacity or cause performance degradation. As shown in Figure 13b, CPU load varied dynamically with task demands, namely, plotting and saving the data periodically, but remained within approximately 60% of available capacity.

For comparison, the Frontiers baseline, known for being a simple and lightweight solution, exhibited  $42.7 \pm 26.2\%$  CPU and  $26.3 \pm 1.2$  RAM usage over 14 runs, showing similar overall resource efficiency.

*c) Execution time and model dimensionality:* Model execution time scaled linearly with model dimensionality (i.e., the number of states considered at each planning step), following:

$$\text{Execution time (s)} \approx 0.18 \times \text{Model dimension} - 2.18.$$

Figure 13a illustrates this relationship, confirming that AIMAPP maintains predictable processing time growth as

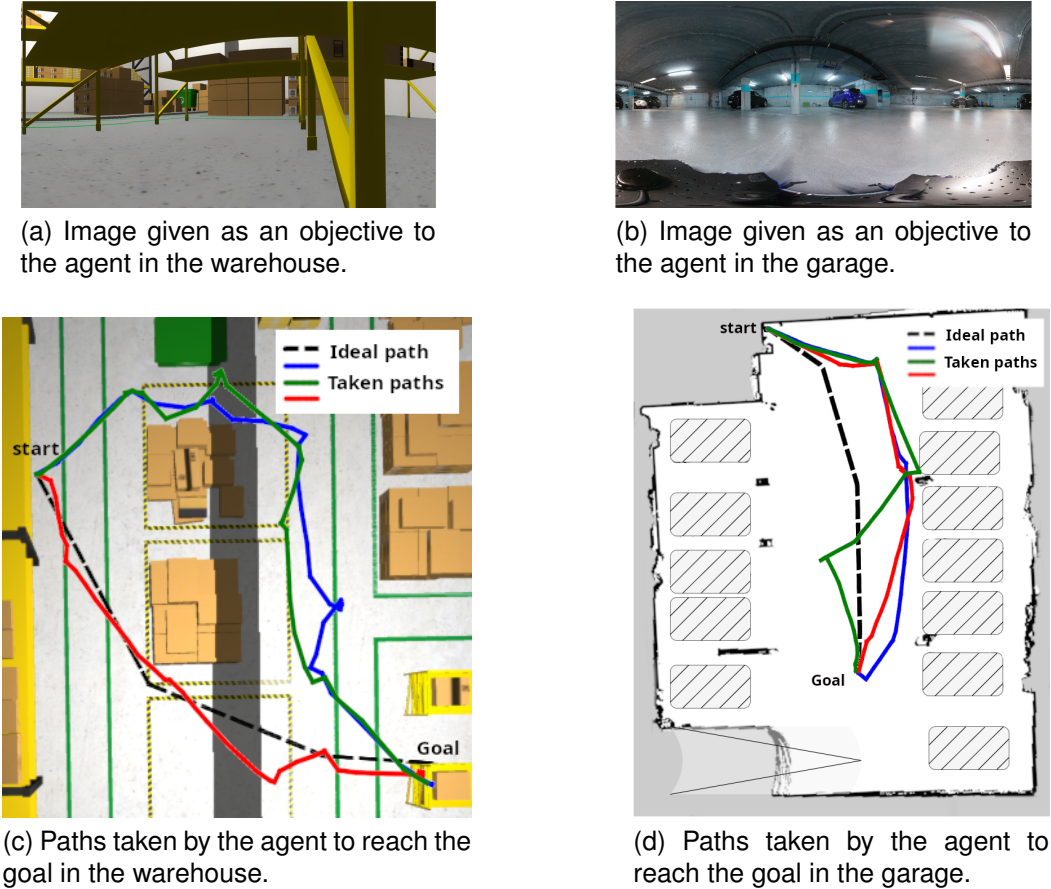


Fig. 12. In the big warehouse and garage, examples of paths taken by the agent (red, green, blue), from the start to the goal image presented along the ideal trajectory (dashed black line).

the model expands. The current configuration used a MCTS depth of 10 (the maximum number of loops, through already explored nodes, to reach a new node without any prior connections), and 30 consecutive simulation runs before deciding on one decisive action, which are both non negligible values that could be reduced to approximately 5 loops and 20 simulations in future iterations to further improve real-time performance.

These results confirm that AIMAPP’s processing time grows linearly with map complexity and computational load remains well within the limits of embedded hardware. No instance of CPU or memory overload was observed, even during extended exploration. Overall system runtime (including motion control and perception pipelines) was not benchmarked, as it depends on the specific robotic platform and sensor suite. The reported measurements isolate the cognitive navigation component, validating its scalability to large and high-dimensional environments without compromising real-time operation.

## VI. DISCUSSION

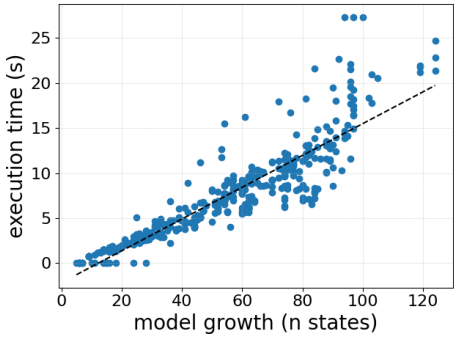
Our results demonstrate that the proposed Active Inference-based model achieves exploration and goal-directed navigation performance. We will recapitulate the key elements here.

*a) Exploration Performance:* AIMAPP achieves exploration efficiency comparable to state-of-the-art planning-based methods such as GBPlanner, FAEL, and Frontier-

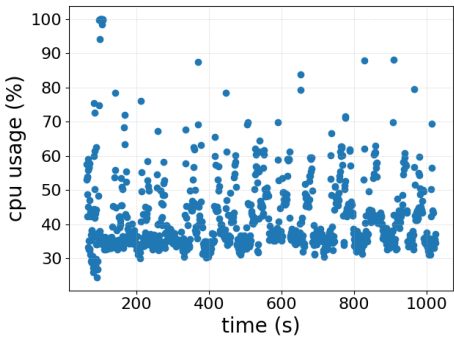
based approaches. In simulated environments, coverage grows smoothly over time, and in real-world deployments, the agent successfully mapped areas up to  $325 \text{ m}^2$ . A key strength of the approach is that it does not rely on heuristic methods as frontiers or pre-defined exploration policies; instead, it evaluates states according to their expected information gain within a generative model of observations and transitions. This enables flexible behaviour in both structured and unstructured spaces.

In our current formulation, the agent reasons over discrete states representing specific locations in a topological graph, with metric information attached for localisation. This design allows efficient planning in large-scale environments but does not explicitly account for the uneven distribution of information across space. For example, a large open hall may be overrepresented in the graph despite containing little new information, whereas a narrow alley may provide greater utility but be collapsed into a few nodes. Grouping states by information gain, as proposed in [58]–[60], could improve the efficiency of both mapping and path planning by reducing redundancy and emphasising high-value regions.

Our system reached complete coverage with trajectories only moderately longer than those of manual exploration (on average 90% as efficient in Coverage Efficiency (CE)). FAEL occasionally outperformed AIMAPP, but at the cost of heavier



(a) Model growth (number of states) impact on execution time (s).



(b) CPU usage in % of the Jetson over runtime (s).

Fig. 13. The measured impact of AIMAPP with MCTS policy evaluation and Nav2 on the Jetson Orin Nano measured over 31 experiments.

3D mapping requirements and less reliable performance, as it failed more than 50% of the time due to various reasons detailed in Appendix D-C. In contrast, AIMAPP and GB-Planner were the most robust baselines among all, with a 79% and 87% success rate, respectively. AIMAPP exploration was considered a failure when the map overlapped too much (localisation was lost and re-localised at the wrong location) or the robot flipped. Gbplanner is proving its reliability by only failing when the robot flips over unconsidered obstacles. Incorporating hierarchical reasoning, as suggested in [30], could further improve performance by enabling the agent to plan over multi-scale representations, accelerating coverage in large open areas while still resolving fine-grained details when necessary.

Overall, the exploration experiments demonstrate that Active Inference provides a competitive alternative to dedicated exploration planners, with the added benefit of being embedded within a single framework that naturally supports goal-directed navigation as well.

*b) Goal-Directed Navigation and Robustness:* The agent consistently reaches visual goals in partially explored environments using belief-driven inference and active planning. Hyperparameters controlling utility, inductive bias, and information gain allow modulation of behaviour depending on the task. While the framework naturally supports mixed objectives simultaneously, we can emphasise reaching a preferred obser-

vation over exploration or vice-versa.

The agent’s goal-directed behaviour balances efficiency with robustness: it often prefers slightly longer paths that offer higher confidence over shorter, more uncertain routes. Replanning is triggered when unanticipated obstacles are encountered or transitions initially deemed feasible turn out to be blocked, ensuring near-optimal performance even in partially explored or dynamic environments. Across all real-world experiments, only two goal-reaching failures were recorded due to extreme drift or physical constraints, demonstrating the system’s reliability.

A key advantage of our approach is the use of probabilistic observation-state mappings, as we can store several observations for the same state, making the model resistant to changes in the environment. However, as environments expand, likelihood distributions for earlier observations naturally dilute, sometimes necessitating revisiting known locations to refresh perceptual beliefs. This reflects the trade-offs of dynamically updating cognitive maps compared to static representations.

Our current implementation uses panoramic visual inputs and a simple SSIM-based processing pipeline. The platform- and sensor-agnostic design ensures adaptability across robotic systems. Incorporating more sophisticated recognition modules (e.g., semantic object detectors [47]) would improve localisation confidence, particularly for critical goal observations. With basic panoramic observations, small modifications in the environment can prevent the agent from recognising the goal at the correct location, highlighting a limitation of the current perception module.

Despite its strengths, our system may fail under extreme environmental changes or definitive sensor loss. In our architecture, in case a sensor fails temporarily, the model pauses until reliable data is available.

Future work include hierarchical reasoning, space chunking based on information gain [58], [59], improving the likelihood model probability dissolution over time and prediction over a long-range horizon [61] and integrating semantic perception for improved goal recognition [47]. These modifications could increase efficiency in exploration and navigation, particularly in large or dynamic environments.

## VII. CONCLUSION

We have presented a biologically inspired, Active Inference-based navigation model that unifies exploration and goal-reaching within a single probabilistic framework. By maintaining a sparse topological map and continuously updating beliefs through sensorimotor feedback, the agent navigates complex, unknown environments without pre-training, metric maps, or heavy reliance on odometry. Experiments in both simulated and real-world settings (up to 325 m<sup>2</sup>) demonstrate performance comparable to state-of-the-art planners, with resilience to sensor drift, ambiguous observations, and dynamic changes.

AIMAPP provides a robust and interpretable navigation solution that integrates exploration and goal-directed behaviour within a unified architecture. It adapts to new environments without training, operates efficiently in varied conditions, and can be seamlessly integrated into existing ROS-based systems.

Its modular, sensor-agnostic design makes it suitable for flexible deployment where task-specific tuning or pre-training is impractical.

Crucially, our approach naturally balances information-seeking and task-driven behaviour, adapting on the fly through probabilistic inference. Its modular, sensor-agnostic design supports interpretability and straightforward integration with existing robotic systems.

Future work should focus on improving goal recognition via richer observation processing [47], enabling user intervention when desired [12], and exploring hierarchical reasoning [30] and spatial chunking [58] to further improve efficiency. Robustness to failing sensors also remains an important direction for deployment in safety-critical settings.

In sum, this work provides evidence that Active Inference can serve as a practical, general-purpose navigation strategy, bridging the gap between neuroscience-inspired models of cognition and the demands of real-world robotic autonomy.

#### ACKNOWLEDGMENTS

This research received funding from the Flemish Government (AI Research Program) under the “Onderzoeksprogramma Artificiële Intelligentie (AI) Vlaanderen” programme and the Inter-university Microelectronics Centre (IMEC).

#### DATA

Our model is available at <https://github.com/decide-ugent/AIMAPP>

#### REFERENCES

- [1] H. S. Hewawasam, M. Y. Ibrahim, and G. K. Appuhamillage, “Past, present and future of path-planning algorithms for mobile robot navigation in dynamic environments,” *IEEE Open Journal of the Industrial Electronics Society*, vol. 3, pp. 353–365, 2022.
- [2] M. Dehghani Tezerjani, M. Khoshnazar, M. Tangestanizade, and Q. Yang, “A survey on reinforcement learning applications in slam,” 07 2024.
- [3] D. de Tinguy, S. Remmery, P. Mazzaglia, T. Verbelen, and B. Dhoedt, “Learning to navigate from scratch using world models and curiosity: the good, the bad, and the ugly,” 2023.
- [4] D. An, H. Wang, W. Wang, Z. Wang, Y. Huang, K. He, and L. Wang, “Etpnav: Evolving topological planning for vision-language navigation in continuous environments,” 2024.
- [5] C. Campos, R. Elvira, J. J. Gomez, J. M. M. Montiel, and J. D. Tardos, “ORB-SLAM3: An accurate open-source library for visual, visual-inertial and multi-map SLAM,” *IEEE Transactions on Robotics*, vol. 37, no. 6, pp. 1874–1890, 2021.
- [6] A. Topiwala, P. Inani, and A. Kathpal, “Frontier based exploration for autonomous robot,” 2018.
- [7] D. S. Chaplot, D. Gandhi, S. Gupta, A. Gupta, and R. Salakhutdinov, “Learning to explore using active neural slam,” in *International Conference on Learning Representations (ICLR)*, 2020.
- [8] T. Parr, G. Pezzulo, and K. Friston, *Active Inference: The Free Energy Principle in Mind, Brain, and Behavior*. The MIT Press, 03 2022.
- [9] K. Friston, R. J. Moran, Y. Nagai, T. Taniguchi, H. Gomi, and J. Tenenbaum, “World model learning and inference,” *Neural Networks*, vol. 144, pp. 573–590, 2021.
- [10] D. de Tinguy, T. Verbelen, and B. Dhoedt, “Learning dynamic cognitive map with autonomous navigation,” *Frontiers in Computational Neuroscience*, vol. 18, Dec. 2024.
- [11] J. Huang, B. Zhou, Z. Fan, Y. Zhu, Y. Jie, L. Li, and H. Cheng, “Fael: Fast autonomous exploration for large-scale environments with a mobile robot,” *IEEE Robotics and Automation Letters*, vol. 8, pp. 1667–1674, 2023.
- [12] T. Dang, M. Tranzatto, S. Khattak, F. Mascarich, K. Alexis, and M. Hutter, “Graph-based subterranean exploration path planning using aerial and legged robots,” *Journal of Field Robotics*, vol. 37, no. 8, pp. 1363–1388, 2020. Wiley Online Library.
- [13] nav2, “nav2,” 2021. Accessed: 2024-12-01.
- [14] H. Wang, C. Wang, and L. Xie, “Lightweight 3-d localization and mapping for solid-state lidar,” *IEEE Robotics and Automation Letters*, vol. 6, no. 2, pp. 1801–1807, 2021.
- [15] F. Shu, J. Wang, A. Pagani, and D. Stricker, “Structure plp-slam: Efficient sparse mapping and localization using point, line and plane for monocular, rgb-d and stereo cameras,” 2023.
- [16] W. Xu, Y. Cai, D. He, J. Lin, and F. Zhang, “FAST-LIO2: fast direct lidar-inertial odometry,” *CoRR*, vol. abs/2107.06829, 2021.
- [17] H. Qin, S. Shao, T. Wang, X. Yu, Y. Jiang, and Z. Cao, “Review of autonomous path planning algorithms for mobile robots,” *Drones*, vol. 7, no. 3, 2023.
- [18] H. Jardali, M. Ali, and L. Liu, “Autonomous mapless navigation on uneven terrains,” *2024 IEEE International Conference on Robotics and Automation (ICRA)*, pp. 13227–13233, 2024.
- [19] S. Sharma, A. Curtis, M. Kryven, J. B. Tenenbaum, and I. R. Fiete, “Map induction: Compositional spatial submap learning for efficient exploration in novel environments,” *CoRR*, vol. abs/2110.12301, 2021.
- [20] Z. D. Guo, S. Thakoor, M. Pflar, B. A. Pires, F. Altché, C. Tallec, A. Saade, D. Calandriello, J.-B. Grill, Y. Tang, M. Valko, R. Munos, M. G. Azar, and B. Piot, “Byol-explore: Exploration by bootstrapped prediction,” 2022.
- [21] D. Shah, B. Eysenbach, G. Kahn, N. Rhinehart, and S. Levine, “Rapid exploration for open-world navigation with latent goal models,” 2023.
- [22] D. Shah and S. Levine, “Viking: Vision-based kilometer-scale navigation with geographic hints,” in *Robotics: Science and Systems XVIII*, Robotics: Science and Systems Foundation, June 2022.
- [23] A. Sridhar, D. Shah, C. Glossop, and S. Levine, “Nomad: Goal masked diffusion policies for navigation and exploration,” 2023.
- [24] R. Mendonca, O. Rybkin, K. Daniilidis, D. Hafner, and D. Pathak, “Discovering and achieving goals via world models,” 2021.
- [25] P. Mirowski, R. Pascanu, F. Viola, H. Soyer, A. J. Ballard, A. Banino, M. Denil, R. Goroshin, L. Sifre, K. Kavukcuoglu, D. Kumaran, and R. Hadsell, “Learning to navigate in complex environments,” *CoRR*, vol. abs/1611.03673, 2016.
- [26] M. Milford, G. Wyeth, and D. Prasser, “Ratslam: a hippocampal model for simultaneous localization and mapping,” in *IEEE International Conference on Robotics and Automation, 2004. Proceedings. ICRA '04. 2004*, vol. 1, pp. 403–408 Vol.1, 2004.
- [27] J. Li, Z. Xu, D. Zhu, K. Dong, T. Yan, Z. Zeng, and S. X. Yang, “Bio-inspired intelligence with applications to robotics: a survey,” *Intelligence and Robotics*, vol. 1, no. 1, 2021.
- [28] R. Kaplan and K. Friston, “Planning and navigation as active inference,” *bioRxiv*, 12 2017.
- [29] M. Zhao, “Human spatial representation: What we cannot learn from the studies of rodent navigation,” *Journal of Neurophysiology*, vol. 120, 08 2018.
- [30] de Tinguy, Daria and Van de Maele, Toon and Verbelen, Tim and Dhoedt, Bart, “Spatial and temporal hierarchy for autonomous navigation using active inference in minigrid environment,” *ENTROPY*, vol. 26, no. 1, p. 32, 2024.
- [31] V. Neacsu, M. B. Mirza, R. A. Adams, and K. J. Friston, “Structure learning enhances concept formation in synthetic active inference agents,” *PLOS ONE*, vol. 17, pp. 1–34, 11 2022.
- [32] S. Nozari, A. Krayani, P. Marin, L. Marcenaro, D. Martín Gómez, and C. Regazzoni, “Exploring action-oriented models via active inference for autonomous vehicles,” *EURASIP Journal on Advances in Signal Processing*, vol. 2024, 10 2024.
- [33] A. Safron, O. Catal, and T. Verbelen, “Generalized simultaneous localization and mapping (g-slam) as unification framework for natural and artificial intelligences: towards reverse engineering the hippocampal/entorhinal system and principles of high-level cognition,” *Frontiers in Systems Neuroscience*, vol. Volume 16 - 2022, 2022.
- [34] J. C. R. Whittington, D. McCaffary, J. J. W. Bakermans, and T. E. J. Behrens, “How to build a cognitive map,” *Nature Neuroscience*, vol. 25, no. 10, pp. 1257–1272, 2022.
- [35] G. Pezzulo, T. Parr, and K. Friston, “Active inference as a theory of sentient behavior,” *Biological Psychology*, vol. 186, p. 108741, 2024.
- [36] K. Friston, T. Fitzgerald, F. Rigoli, P. Schwartenbeck, J. O. Doherty, and G. Pezzulo, “Active inference and learning,” *Neuroscience and Biobehavioral Reviews*, vol. 68, pp. 862–879, 2016.

- [37] M. Rosenberg, T. Zhang, P. Perona, and M. Meister, “Mice in a labyrinth show rapid learning, sudden insight, and efficient exploration,” *eLife*, vol. 10, p. e66175, jul 2021.
- [38] C. B. Browne, E. Powley, D. Whitehouse, S. M. Lucas, P. I. Cowling, P. Rohlfshagen, S. Tavener, D. Perez, S. Samothrakis, and S. Colton, “A survey of monte carlo tree search methods,” *IEEE Transactions on Computational Intelligence and AI in Games*, vol. 4, no. 1, pp. 1–43, 2012.
- [39] Z. Fountas, N. Sajid, P. A. M. Mediano, and K. Friston, “Deep active inference agents using monte-carlo methods,” 2020.
- [40] K. J. Friston, T. Salvatori, T. Isomura, A. Tschantz, A. Kiefer, T. Verbeelen, M. Koudahl, A. Paul, T. Parr, A. Razi, B. Kagan, C. L. Buckley, and M. J. D. Ramstead, “Active inference and intentional behaviour,” 2023.
- [41] D. George, R. Rikhye, N. Gothoskar, J. S. Guntupalli, A. Dedieu, and M. Lázaro-Gredilla, “Clone-structured graph representations enable flexible learning and vicarious evaluation of cognitive maps,” *Nature Communications*, vol. 12, 04 2021.
- [42] M. Peer, I. K. Brunec, N. S. Newcombe, and R. A. Epstein, “Structuring knowledge with cognitive maps and cognitive graphs,” *Trends in Cognitive Sciences*, vol. 25, no. 1, pp. 37–54, 2021.
- [43] P. Foo, W. Warren, A. Duchon, and M. Tarr, “Do humans integrate routes into a cognitive map? map- versus landmark-based navigation of novel shortcuts.,” *Journal of experimental psychology. Learning, memory, and cognition*, vol. 31, pp. 195–215, 04 2005.
- [44] R. Epstein, E. Z. Patai, J. Julian, and H. Spiers, “The cognitive map in humans: Spatial navigation and beyond,” *Nature Neuroscience*, vol. 20, pp. 1504–1513, 10 2017.
- [45] W. H. Warren, D. B. Rothman, B. H. Schnapp, and J. D. Ericson, “Wormholes in virtual space: From cognitive maps to cognitive graphs,” *Cognition*, vol. 166, pp. 152–163, 2017.
- [46] M. Milford, “Vision-based place recognition: how low can you go?,” *The International Journal of Robotics Research*, vol. 32, no. 7, pp. 766–789, 2013.
- [47] D. S. Chaplot, D. Gandhi, A. Gupta, and R. Salakhutdinov, “Object goal navigation using goal-oriented semantic exploration,” 2020.
- [48] V. S. Dorbala, J. F. Mullen, and D. Manocha, “Can an embodied agent find your “cat-shaped mug”? ILM-based zero-shot object navigation,” *IEEE Robotics and Automation Letters*, vol. 9, p. 4083–4090, May 2024.
- [49] aws-robotics, “aws-robomaker-small-warehouse-world,” 2020. Accessed: 2024-08-01.
- [50] aws-robotics, “aws-robomaker-small-house-world,” 2021. Accessed: 2024-10-01.
- [51] P. Gyanani, M. Agarwal, R. Osari, *et al.*, “Autonomous mobile vehicle using ros2 and 2d-lidar and slam navigation,” *Research Square*, vol. Preprint (Version 1), May 2024. Available at Research Square.
- [52] M. Tranzatto, M. Dharmadhikari, L. Bernreiter, M. Camurri, S. Khattak, F. Mascarich, P. Pfreundschuh, D. Wisth, S. Zimmermann, M. Kulkarni, V. Reijgwart, B. Casseau, T. Homberger, P. D. Petris, L. Ott, W. Tubby, G. Waibel, H. Nguyen, C. Cadena, R. Buchanan, L. Wellhausen, N. Khedekar, O. Andersson, L. Zhang, T. Miki, T. Dang, M. Mattamala, M. Montenegro, K. Meyer, X. Wu, A. Brod, M. Mueller, M. Fallon, R. Siegwart, M. Hutter, and K. Alexis, “Team cerberus wins the darpa subterranean challenge: Technical overview and lessons learned,” 2022.
- [53] H. Oleynikova, Z. Taylor, M. Fehr, J. I. Nieto, and R. Siegwart, “Voxblox: Building 3d signed distance fields for planning,” *CoRR*, vol. abs/1611.03631, 2016.
- [54] D. Duberg and P. Jensfelt, “UFOMap: An efficient probabilistic 3D mapping framework that embraces the unknown,” *IEEE Robotics and Automation Letters*, vol. 5, no. 4, pp. 6411–6418, 2020.
- [55] clearpathrobotics, “Jackal.” Accessed: 2025-07-28.
- [56] husarion, “rosbotxl.” Accessed: 2025-07-28.
- [57] H. Xu, P. Baracskay, J. O’Neill, and J. Csicsvari, “Assembly responses of hippocampal ca1 place cells predict learned behavior in goal-directed spatial tasks on the radial eight-arm maze,” *Neuron*, vol. 101, no. 1, pp. 119–132.e4, 2019.
- [58] A. Caticha, “The information geometry of space and time,” 2005.
- [59] J. Hwang, Z.-W. Hong, E. Chen, A. Boopathy, P. Agrawal, and I. Fiete, “Grid cell-inspired fragmentation and recall for efficient map building,” 2024.
- [60] M. Selin, M. Tiger, D. Duberg, F. Heintz, and P. Jensfelt, “Efficient autonomous exploration planning of large-scale 3-d environments,” *IEEE Robotics and Automation Letters*, vol. 4, no. 2, pp. 1699–1706, 2019.
- [61] W. W. L. Nijhut, M. Lukashchuk, T. van de Laar, and B. de Vries, “A message passing realization of expected free energy minimization,” 2025.

## APPENDIX A

### MODEL DEFINITION

#### A. Model Parameters

This section details the parameters used to configure and operate our active inference-based navigation model. These parameters define the structure of the agent’s internal representation, the characteristics of the planning process, and the learning dynamics that allow it to adapt to environmental changes.

At initialisation, a series of hyperparameters can be set. The user can define :

- the number of likelihood matrices the agent will use, in our paper, we set it to two, for the visual and pose likelihood matrices. Theoretically, it can be increased to accept more observations, such as Lidar or Radar, etc., but it was not tested here.
- the number of available actions, discretised over the agent’s rotation or movement space (typically 360°). When the given number is odd, an additional “stay” or “no-op” action is included. In this paper, it was set to 13 actions.
- the physical radius of the agent, acting as a collision buffer when deciding whether new states can be created near obstacles.
- the influence radius, which defines the minimum distance required between states. If the agent moves within this radius, no new topological node is created, promoting compactness in the map. In our experiment, it was set to 1m in small environments (real home and mini-warehouse) and 2m in larger environments ( $> 40m^2$ ).
- how far the agent can see, or how many new, consecutive nodes can be hypothesised within the current LiDAR sensing range, enabling more anticipatory map expansion during exploration. In this paper, a maximum of 8 nodes was set.

#### 1) Transition Update:

$$B_\pi = B_\pi + Q(s_t | s_{t-1}, \pi) Q(s_{t-1}) * B_\pi * \lambda \quad (9)$$

To update its beliefs about the environment, the agent uses a Dirichlet-based pseudo-count mechanism (Equation 9) with situation-dependent learning rates ( $\lambda$ ). These rates vary based on whether the agent:

- successfully reaches a location,
- is physically blocked while trying to move,
- or anticipates reaching (or failing to reach) a location based on sensory evidence.

Table III lists the specific learning rates for each situation. This continual adjustment allows the agent to refine transition likelihoods in its internal model rapidly.

TABLE III  
TRANSITION LEARNING RATE ( $\lambda$ ) DEPENDING ON THE SITUATION

Transitions	Possible	Impossible	Predicted Possible	Predicted Impossible
Forward	7	-7	5	-5
Reverse	5	-5	3	-3

2) *Uncertainty About Current State*: To determine whether an agent is lost, we evaluate its certainty about the current state. Specifically, we compute a Z-score to measure how strongly the most likely state stands out compared to the others. If this dominance falls below a user-defined threshold (set to 4 in this work), the agent is considered uncertain about its location.

### B. Expected Free Energy Terms

$H$  is an inductive term applied to the state preference  $C_s$  defined in Equation 10, which is computed inductively by propagating backwards in time from the goal state toward the current state (in  $n$  steps, that might be lower than the planning horizon). This inductive process accumulates structural preferences and becomes silent (i.e., has no influence) if no specific target state is preferred or if the preferred state lies beyond the predictive horizon. Let  $C_{s_0}$  be a weighted preference vector over existing states, as derived from the joint preference over observations ( $C_o$ ) and transitions ( $C_p$ ). Then the backwards recursion is defined as [40]:

$$\begin{aligned} C_{s_n} &= B_s^T \odot C_{s_{n-1}} \quad \text{for } n = 0, \dots, \tau \\ H &= \ln(\epsilon) \cdot (B_s^T \odot C_{s_\tau}) \odot s(\tau) \end{aligned} \quad (10)$$

$n$  is a backwards value propagating from the goal (thus the future, if under our prediction horizon) up to our current state  $t$ , if  $C_s$  lies over the horizon, we can predict, this term will also be silent.

### C. Monte Carlo Tree Search

We use an MCTS merged with Active Inference to determine the expected free energy of the surrounding possible paths. MCTS is used to explore possible future trajectories as far as possible while avoiding the limitations of fixed policy sets typically used in standard Active Inference implementations.

In many Active Inference models, policies are predefined and limited in number, with the agent selecting among them by evaluating their expected free energy at each decision point [10], [28], [31]. This fixed policy set constrains the agent's ability to flexibly adapt to complex, dynamic, or large-scale environments, as it cannot reason beyond the span of those precomputed policies.

By contrast, integrating MCTS allows the agent to dynamically simulate multiple future action sequences (i.e., rollouts) from its current belief state. These simulations are guided by the principle of minimising expected free energy [39], enabling the agent to actively search for policies that balance goal-directed behaviour (utility maximisation) with epistemic exploration (information gain). This approach enables deeper lookahead without incurring the combinatorial explosion of evaluating all possible action sequences, thus significantly reducing computational load while maintaining adaptive and scalable planning.

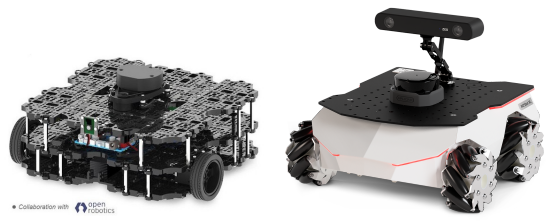
Moreover, using MCTS with Active Inference enables the agent to flexibly revise its planned trajectory in light of new evidence at each time step, rather than being bound by a fixed horizon or static policy set. This results in more robust and

context-sensitive navigation behaviour, particularly in uncertain or partially observable environments. Our algorithm is presented in Algorithm 1, where the policy length sets the number of future steps we need to predict, the lookahead policy is the depth of the agent's policy simulation horizon (set to 10 in our experiments), and the possible motions are the actions the agent can execute from its current position.

Two parameters are used, the lookahead policy, which is represented as  $n$  in H equation 10 (how far from us can the goal be induced), and the policy length that determine how many time we run the planning (it will impact how far we can see, while not setting a strict rule on horizon visibility), we set it to one action. For each step in the policy length, we run the MCTS simulation 30 times before determining which action is the most ideal.

## APPENDIX B ROBOTS

Our system is robot-agnostic; however, we have to adapt the sensor pipeline to the specific sensors used. In simulation, we used a TurtleBot3 Waffle with a Pi camera and a 360-degree lidar with a 12 m range. In the real environment, several robots have been used; at first, we used the Turtlebot with a forward lidar of 240 degrees of 12 m range and a camera RealSense D435; the Turtlebot4 with a 360-degree lidar of 8 m range and a camera OAK-D-Pro. Due to a large uncorrected drift (1m drift after a 3m motion), the resulting maps did not allow a clear superposition with the layout of the environment; thus, we used a RosbotXL with a 360-degree lidar of 18m range and a 360-degree camera (Theta X) to better show the results of the navigation. However, while the Lidar range is 18m, the agent only considers the Lidar up to 8 consecutive nodes as defined in Appendix A-A to create or update new transitions to be as reliable as possible.



(a) Turtlebot3: Waffle (b) Husarion: RosbotXL

Fig. 14. Turtlebot3 waffle robot was used in simulation, while tests have been conducted with a turtlebot and RosbotXL in the real environment

**1 Algorithm:** AIF based MCTS

```

Input: possible_motions, policy_length, lookahead_policy, num_simulation
Output: best policy
2 Function MCTS planning (possible_motions, policy_length, lookahead_policy, num_simulation) :
3   qs  $\leftarrow$  get believed localisation over states() ;
4   qo  $\leftarrow$  get expected observations for qs(qs) ;
5   root  $\leftarrow$  create root state(qs, qo, possible_motions);
6   for i  $\leftarrow$  1 to policy_length do
7     for i  $\leftarrow$  1 to num_simulation do
8       leaf  $\leftarrow$  Selection(root);
9       expanded_leaf  $\leftarrow$  Expansion(leaf);
10      reward  $\leftarrow$  Simulation(expanded_leaf, lookahead_policy);
11      Backpropagate(expanded_leaf, reward);
12      actioni  $\leftarrow$  SelectBestAction(root);
13      root  $\leftarrow$  leaf;
14      selected actions  $\leftarrow$  actioni
15   return selected actions;
16 Function Selection (node) :
17   while node has children do
18     node  $\leftarrow$  child of node with highest UCB1 score;
19   return node ;
20 Function Expansion (node) :
21   foreach action in node.possible_actions do
22     next_pose  $\leftarrow$  Transition(node.pose, action);
23     next_pose, qs', qo', G  $\leftarrow$  Infer (node.qs, action);
24     Create new child node with state (qs', next_pose, qo', G) ;
25   return node ;
26 Function Simulation (node, lookahead_policy) :
27   foreach action in node.possible_actions do
28     action  $\leftarrow$  choice from node actions;
29     next_pose, qs', qo', G  $\leftarrow$  Infer (qs, action, lookahead_policy);
30     if best measured G then
31       best_G  $\leftarrow$  G;
32     total_reward  $\leftarrow$  total_reward + best_G;
33   return total_reward ;
34 Function Backpropagate (node, reward) :
35   while node exists do
36     node  $\leftarrow$  update node(node, reward);
37     node  $\leftarrow$  node.parent;
38 Function SelectBestAction (root) :
39   foreach (a, child) in root.childs do
40     Compute average reward of child;
41   return action action with highest AIF policy score ;
42 Function Infer (qs, action) :
43   next_pose  $\leftarrow$  Transition(pose, action);
44   qs'  $\leftarrow$  BeliefTransition(qs, action);
45   qo'  $\leftarrow$  ExpectedObservation(qs');
46   G  $\leftarrow$  ExpectedFreeEnergy(qs', qo', qs, action);
47   return next_pose, qs', qo', G ;

```

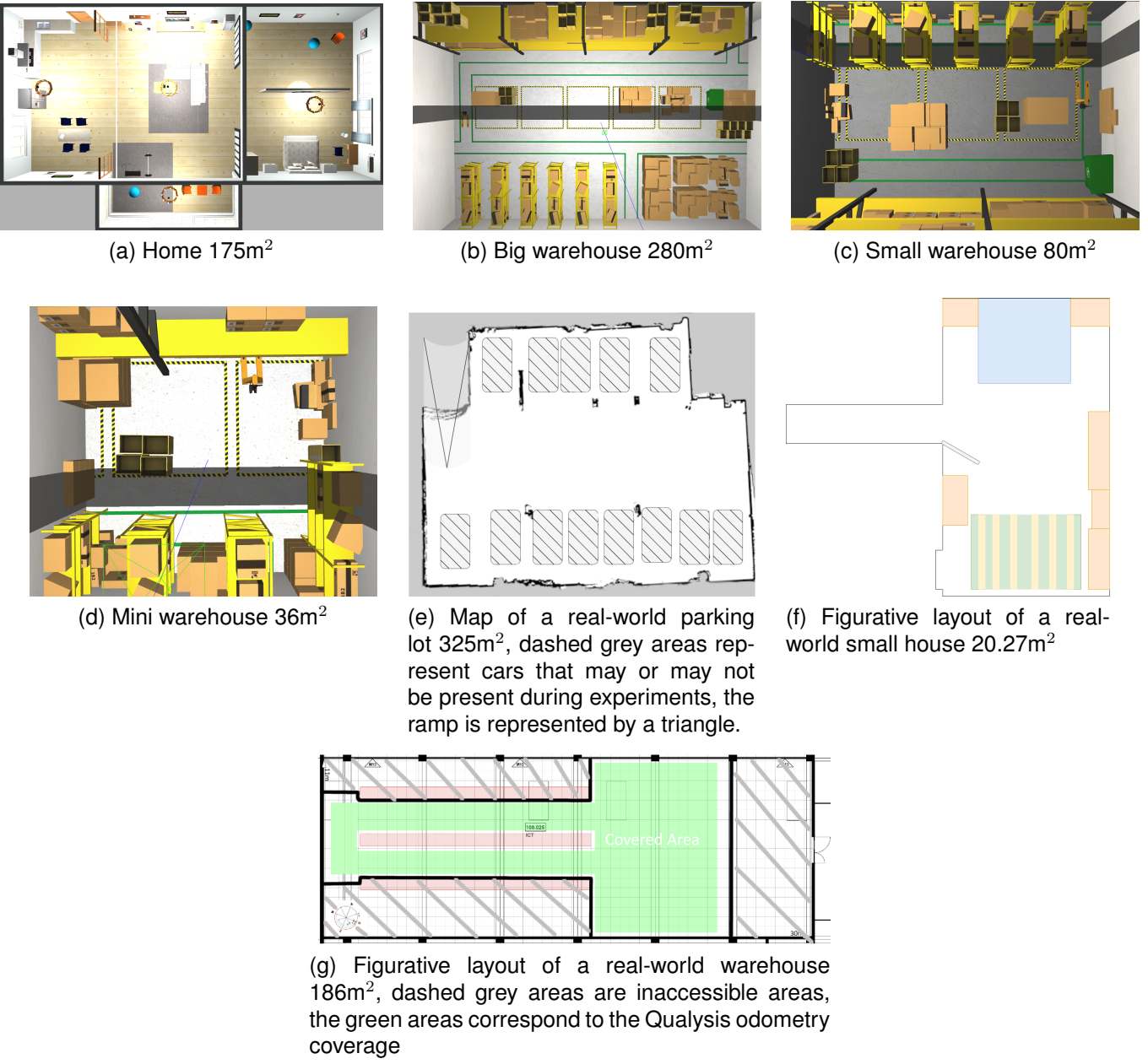


Fig. 15. The three Amazon warehouse environments and the house used in Gazebo, as well as the parking lot, small house and warehouse used in the real world.

## APPENDIX C ENVIRONMENTS

Our experiments used a home [50] of 156m<sup>2</sup> and a warehouse [49] of 3 different sizes, ranging from 36m<sup>2</sup>, 80m<sup>2</sup> up to 280<sup>2</sup> and a real-world house of 21m<sup>2</sup>, a warehouse of 185m<sup>2</sup> and a parking lot of 325m<sup>2</sup>. All environments are presented in Figure 15.

## APPENDIX D DETAILS ABOUT EXPERIMENTAL RESULTS

### A. Aversial Models

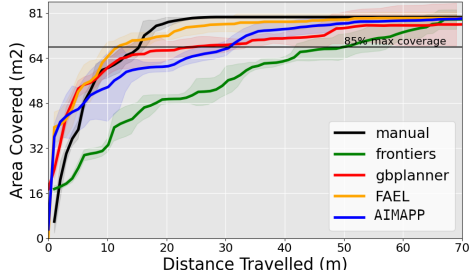
GBPlanner, FAEL, and Frontiers were used with their given parameters, except for the map resolution, which was increased

to 0.05m/cell. Other parameters, such as obstacle inflation, were modified to ensure that all agents could physically reach every location.

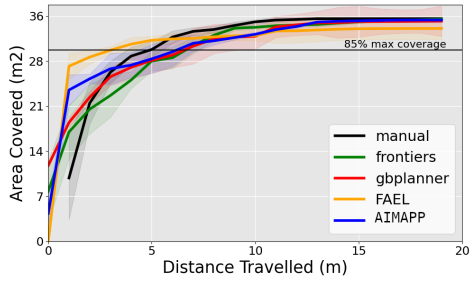
Despite our efforts, FAEL wouldn't fully turn around the central box in the mini warehouse, explaining why Figure 16b coverage is not 100%.

### B. Exploration paths

In smaller environments (warehouses up to 80m<sup>2</sup>), model efficiency is more closely aligned across different approaches, as can be seen in Figure 16 and matches the five averaged manual explorations realised from the same starting points, metrical results are summarised in Table IV. This homogeneity between models is largely due to the limited Lidar range,



(a) Coverage of the small warehouse by Frontiers, Gbplanner, FAEL and AIMAPP, over the travelled distance. Obstacles were removed from the total map area ( $80\text{m}^2$ )



(b) Coverage of the mini warehouse by Frontiers, Gbplanner, FAEL and AIMAPP, over the travelled distance. Obstacles were removed from the total map area ( $36\text{m}^2$ )

Fig. 16. Coverage efficiency of each model over 5 runs in small environments, considering the agent's travelling distance.

TABLE IV  
EXPLORATION EFFICIENCY METRICS ACROSS ENVIRONMENTS. CE: COVERAGE EFFICIENCY ( $\text{m}^2/\text{m}$ ), NAUC: NORMALISED AREA UNDER COVERAGE CURVE. VALUES ARE MEAN  $\pm$  STD OVER 5 RUNS.

Env.	Model	CE	nAUC
Small Warehouse	Manual	$3.13 \pm 0.43$	$0.74 \pm 0.03$
	AIMAPP	$2.25 \pm 0.87$	$0.87 \pm 0.04$
	Frontiers	$1.08 \pm 0.12$	$0.73 \pm 0.03$
	FAEL	$2.60 \pm 0.58$	$0.98 \pm 0.03$
	GBPlanner	$1.59 \pm 0.25$	$0.63 \pm 0.06$
Mini warehouse	Manual	$2.66 \pm 0.16$	$0.92 \pm 0.01$
	AIMAPP	$2.64 \pm 0.98$	$0.91 \pm 0.04$
	Frontiers	$2.45 \pm 0.07$	$0.88 \pm 0.01$
	FAEL	$2.61 \pm 1.16$	$0.85 \pm 0.03$
	GBPlanner	$2.55 \pm 0.4$	$0.82 \pm 0.08$
Real Garage	Manual	13.18	0.74
	AIMAPP	$7.41 \pm 0.87$	$0.71 \pm 0.03$

which can quickly encompass a significant portion of the environment, thereby reducing the relative advantage of long-term planning strategies.

Example of exploration trajectories from AIMAPP, FAEL, GBPlanner, and a Frontier-based approach are illustrated in Figure 17, all starting from the same initial location near the dumbbell (trajectory colour progresses from black to yellow). In this run, FAEL, AIMAPP, and Frontiers all achieved nearly 100% coverage, while GBPlanner reached approximately 95%.

Notably, GBPlanner became trapped near the chair in the sports room, preventing complete exploration.

Qualitatively, the strategies exhibit distinct behaviours. FAEL avoided entering the playroom but approached its doorway, providing partial coverage of the interior without direct visitation. The Frontier-based strategy aggressively targeted the largest unexplored areas, ensuring complete coverage but at the cost of repeated backtracking and long, inefficient paths, an approach that does not scale well to larger environments. AIMAPP exhibited a mixture of forward progression and small corrective loops to accumulate additional observations. However, in this run, it failed to detect that the bedroom could be accessed from the playroom on the far right, leaving this connection unexplored.

These results highlight that while coverage performance across models converges in smaller environments, qualitative differences in trajectory efficiency and robustness become more apparent in larger, more complex spaces.

Direct coverage comparisons between AIMAPP and FAEL or GBPlanner could not be performed in real-world settings due to incompatible sensor requirements. In addition, our evaluation pipeline relies on Nav2 to generate a 2D occupancy map from Lidar measurements for metric calculation. This introduces a limitation: in real-world house exploration, coverage values were fundamentally unreliable due to significant drift and restricted Lidar range. For the same reason, Frontier-based results in the garage could not be fairly compared to our model. In these cases, Nav2 failed to compensate for wheel slippage and drift (e.g., when the robot became stuck on sandy ground), which resulted in superimposed, misaligned maps that could not be disambiguated post hoc.

To provide a consistent baseline, all reported real-world coverage values for AIMAPP were averaged over five runs and compared to the coverage obtained through manual exploration using Nav2 SLAM mapping. The achieved coverage in the parking lot environment by AIMAPP and our manual teleoperation is illustrated in Figure 18. It is worth noting that the accessible area varied between runs, as parked cars dynamically altered the free space available to the agent. Despite these variations, AIMAPP demonstrated robust exploration and reliable coverage across multiple trials.

### C. Reasons for human interventions

TABLE V  
NUMBER OF TIMES THE ROBOT GOT STUCK AND REQUIRED INTERVENTION PER ENVIRONMENT.

External intervention	AIMAPP	FAEL	Gbplanner	Frontiers
Home	2	5	1	5
Big warehouse	0	5	2	0
Small warehouse	1	3	4	2
Mini warehouse	0	2	2	3
Real home	4	x	x	x
Real parking	2	x	x	x
Real warehouse	7	x	x	14

The reasons for human interventions varied substantially across models:

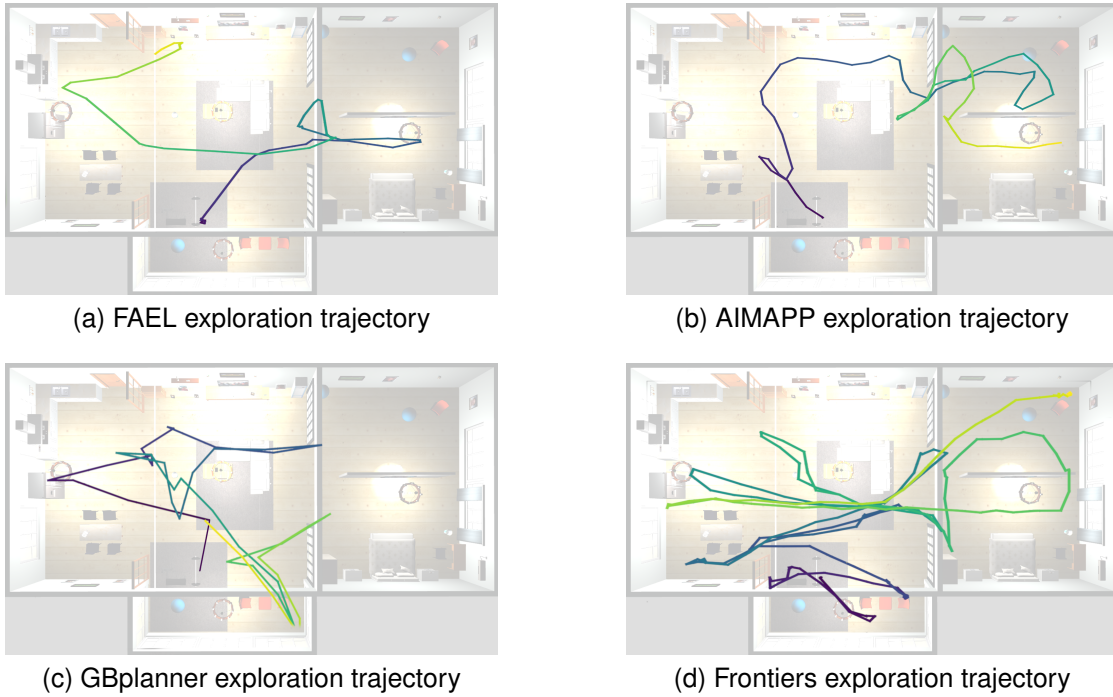


Fig. 17. Approximate exploration trajectories from black to yellow. We can notice how some agents never enter the bedroom and playroom, as their Lidar range can already encompass most of it from the doors (yet the coverage would not be fully complete).

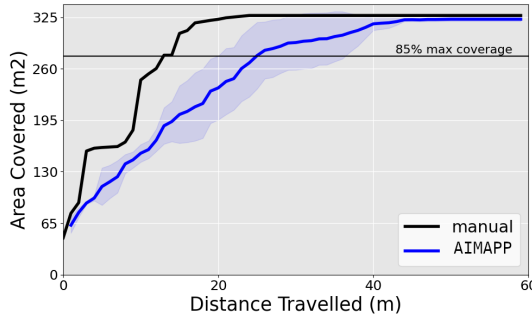


Fig. 18. Coverage of the real-world parking lot by AIMAPP compared to a manual exploration. Note that the accessible areas vary between runs due to the presence of cars.

**AIMAPP:** Most interventions occurred when the LiDAR failed to detect certain obstacles, such as forklifts or flat-based chairs. In these cases, the robot would either collide too quickly and flip over or remain stuck. Since Frontiers uses the same LiDAR, it experienced similar issues. For both models, this limitation could theoretically be mitigated by inflating obstacle areas in the costmap when using Nav2; however, doing so would also significantly restrict the explorable space, making coverage comparisons unfair. In the real warehouse, we also had the issue of undetected white walls (the lidar would give an erroneous distance). When against an undetected obstacle, the robot would have its wheels spinning against the wall, updating the odometry. Thus, the agent did not receive the information that the robot was stuck. We had to send the motion planning failure manually to the agent and push the robot away from the obstacle. Another situation has

been a manual re-localisation of the robot when the drift was too big in an unexplored area, leading to a non-sensical map from a human perspective (the map was valid for the model, but could not be used for the benchmarking).

**Frontiers:** In addition to the LiDAR issue, Frontiers often persevered in attempting to reach unreachable goals, repeatedly trying to navigate toward them regardless of feasibility. When this happened, the agent was manually repositioned to a more central area, allowing exploration to resume.

**FAEL:** Failures were typically linked to mismatches between topological node creation and obstacles in Voxblox. If a node was generated just before the obstacle was considered by its sensors, FAEL could repeatedly attempt to reach it and remain stuck. A gentle push usually allowed the agent to continue, similar to Frontiers (unsurprising given FAEL’s frontier-based logic). FAEL also exhibited failures in open spaces, where its open-space detection module occasionally misclassified the surroundings as non-traversable (see Figure 19). Again, slight repositioning often resolved the issue. However, sometimes, the agent would just persevere in refusing to move for undefined reasons, requiring to cancel the exploration and start anew.

**GB-Planner:** This model proved more robust to both obstacle occlusion and sensor noise, successfully detecting objects such as forklifts and chairs. However, GB-Planner did not always classify these obstacles as impassable. When a goal lay beyond such objects, the planner frequently generated a direct path across them, while it was, in fact, an infeasible trajectory. Since no automatic fail-safe is in place, the agent remained blocked until manually nudged aside, which then triggered re-planning around the obstacle.

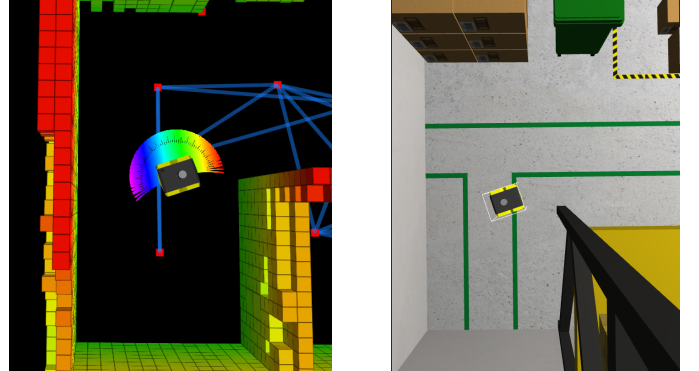
It is worth noting that in our framework, re-planning when faced with an undetected obstacle is handled not by the decision-making component itself but by the motion planning layer. The model simply specifies the target objective and relies on the motion planner to report its current position and whether it is moving successfully.

Finally, in the real-world parking lot experiments, interventions required to move the robot away from approaching cars were not included in Table V, as we halted the experiment in such situations.

Every model had cases of failure that even human intervention could not resolve (usually, if the robot tilted too much, the Lidars would form an inconsistent map, and the agent would struggle to recover from it). The details of the success rate to obtain five successful explorations is reported in Table VI. Frontiers succeeded in its exploration in only 52% of the runs overall. Largely due to Nav2 losing the odometry or the SLAM merging aisles together. FAEL has an even lower rate of 48% successful runs. The exploration strategy is efficient when everything works well, but sometimes the model refuses to start or stops in an open space, and even moving it a bit or waiting does not solve the situation. We have a 79% success rate. In our case, the robot failed due to the robot flipping and wheels still recording motion or the agent being temporarily lost and re-localising at the wrong position, proposing a scrambled map. In the real world, we could pause the agent to solve sensor issues (namely, a loose wheel, resetting the Lidar or restarting the robot) and resume the runs without considering it a failure, a feature that would be missing in most models. Gbplanner is the most robust model with an 87% success rate; failure only resulted from the agent not considering an obstacle insurmountable and flipping the robot, resulting in a scrambled 3D map.

TABLE VI  
PERCENTAGE OF EXPLORATION SUCCESS RATE FOR EACH MODEL OVER  
EACH ENVIRONMENT.

External intervention	AIMAPP	FAEL	Gbplanner	Frontiers
Home	0.71	0.45	0.83	0.63
Big warehouse	1	0.5	1	0.83
Small warehouse	1	0.63	0.87	0.83
Mini warehouse	0.83	0.83	1	0.83
Real home	0.6	x	x	0.09
Real parking	0.75	x	x	0.00
Real warehouse	0.63	x	x	0.45



(a) Detected free space around the agent is rainbow coloured while actual free space is black.  
(b) Jackal in the environment

Fig. 19. Example of the FAEL getting stuck in an open area.